Aalborg University
Department of Energy Technology

PV2GRID

A next generation grid side converter with advanced control and power quality capabilities

Final Report (Project No.: 2015-1-12359**)**

Frede Blaabjerg, Professor
Yongheng Yang, Assistant Professor

24-Nov-17

Period:

Three years (201502-201801)

Participants at AAU:

Frede Blaabjerg (Prof.), Yongheng Yang (Asst. Prof.), and Ariya Sangwongwanich (Ph.D. student)

Consortium:

Aalborg University (AAU)

University of Cyprus (UCY)

Quantum Corporation (not funded)

Sponsors:

This project was supported in part by the European Commission within the European Union's Seventh Framework Program (FP7/2007–2013) through the SOLAR-ERA.NET Transnational Project (PV2.3-PV2GRID), by Energinet.dk (ForskEL, Denmark, Project 2015- 1-12359), and in part by the Research Promotion Foundation (RPF, Cyprus, Project KOINA/SOLAR-ERA.NET/0114/02).

1. Project details

Project title	A next generation grid side converter with advanced control and power quality capabilities
Project identification (program abbrev. and file)	PV2GRID, 2015-1-12359
Name of the programme which has funded the project	SOLAR-ERA.NET Transnational Project – PV2.3
Project managing company/institution (name and address)	Aalborg University Department of Energy Technology Pontoppidanstraede 111, 9220 Aalborg East, Denmark
Project partners	University of Cyprus (UCY) Quantum Corporation (QUANTUM)
CVR (central business register)	DK 29 10 23 84
Date for submission	24-11-2017

2. Short description of project objective and results

Objectives: Grid side converter (GSC) is the key for the photovoltaic (PV) integration. GSCs are still not capable of advanced control features that enable the full control of PV systems, e.g., with fault ride through, reactive power support, and power generation control. This project aims to develop a next-generation GSC with advanced control and novel operational mode capabilities, in order to further reduce the cost of PV energy.

Results: A 6-kW prototype of grid-side converters with advanced control functionalities has been developed and practically implemented at Aalborg University (AAU), which is a single-phase PV system. Various advanced control and operational modes have been implemented and tested on the system. A similar prototype with three-phase grid-connected PV systems has been developed at the University of Cyprus, where similar control functionalities have been realized on three-phase systems.

3. Executive summary

Several goals have been set at international and European levels regarding the energy and climate change of the planet. According to the European Union, these objectives are well known as the "20-20-20" targets by 2020, which requires that 20% of energy consumption is produced from Renewable Energy Sources (RES), a reduction of 20% in greenhouse gas emissions and an improvement of 20% in energy efficiency. Higher goals are being set for 2030 (27%, 40%, and 30%, respectively). This project focuses on the large-scale deployment of photovoltaic (PV) systems through improving their grid integration. The driving forces of this ambitious project focus on three issues of critical significance that inhibit the massive deployment of PVs:

a) Variable and environmental-dependent nature of PV generation;
b) Problems associated with a massive deployment of distributed generation (e.g., grid unbalance, harmonics); and
c) Need to develop appropriate fault ride through (FRT) solutions to allow them to support the grid during faults.

It is expected that the project results and products will address the challenges and achieve the objectives with regards to the grid interconnection and the large-scale deployment of PV systems as set by the implementation plan of the Solar Europe Industry Initiative (SEII).

The most crucial point with regards to the grid integration of PV systems is the grid side converter (GSC) which is based on power electronic technology. GSCs are still not capable of advanced control features that enable the full control of RES with FRT capabilities, reactive power support, and generation control. The major objective of this project is to develop a next-generation GSC (one for single- and one for three- phase systems) with advanced control and novel operational mode capabilities, which will benefit all stakeholders of PV systems in terms of:

a) A seamless integration of PV systems in the power grid
b) A further larger scale deployment of PV systems due to the several advantages of the new converters
c) Possibilities to extend the GSC technology to other green technologies
d) Maximization of the utilization of PV systems to improve the power system operation
e) Increase of the incomes/returns from a solar energy investment for a self-sustainable market of PV systems.

The GSCs designed and developed in this project will achieve an improved performance ensuring the proper grid integration of PV systems under any grid conditions. Additionally, the new GSCs will be enhanced with novel operational functionalities that will allow new operating approaches. The new operating modes will contribute to the development of multifunctional industrial products that can be used for the grid integration of several new technologies with emphasis on PV systems. The novel operational functionalities of the GSC will pave the way for a higher penetration of solar energy and will maximize the utilization of PV systems to:

- Enhance the value and increase the competiveness of PV systems
- Maximize the income of a solar project for a self-sustainable market of PV systems
- Enhance the stability and reliability of power systems
- Improve the power quality and minimize power losses of Distribution Networks (DN)

The project will clearly benefit the PV industry, the power system operator at distribution and transmission level, the investors on PV systems, the electricity consumer, and the environment. A cost-effective and smooth integration of considerably more PV systems will be achieved.

The successful completion of the project is guaranteed due to world-class/pioneer partners of a balanced and complementary consortium. The partners combine great expertise on the following areas: development of advanced methodologies for GSC, design and reliability of power electronics, and power system operation/power quality/stability and investment on energy market. The result of the project can be used to enable partners to enter into the PV industry by commercializing the results on novel single- and three-phase inverters for PV systems.

4. Project objectives

Project objective: This project aims to advance the technology related to the seamless grid integration of photovoltaic (PV) systems. Next generation power electronic Grid Side Converters (GSC) will be developed within this project with advanced capabilities and innovative operational management approaches. Therefore, the new GSC with novel operational modes can contribute to the progress of PV systems, by advancing the follow Key Performance Indicators (KPI) as defined by the Solar Europe Industry Initiative (SEII):

-enable multifunctional products
-increase PV competitiveness
-voltage and reactive power control
-power quality enhancement of PV systems

-increase flexibility of power system
-enable congestion management
-decrease of network losses
-decrease peak demand ratio

Additionally, the proposed GSC for PV systems can also contribute to achieve the below goals:

-maximize the value of PV systems
-enable a high penetration of PV systems
-enhance the economic benefit of the prosumers
-provide support to the Distribution Network
-symmetrize the loads among the three phases
-decrease the electricity price for the consumers

The consortium consists of experts in the design of GSC controllers for the proper grid-connection of PV systems. The project aims at developing new GSC controllers for single- and three-phase PV systems with advanced synchronization methods, enhanced current controllers and novel active and reactive power (PQ) controllers for the proper operation of PV systems under harmonic distorted environment, unbalanced conditions, and grid faults. Novel operational approaches for the GSC are also proposed in this project, where the GSC of the PV system is utilized in a way to symmetrize (balance) the load among the three phases in the DN, to compensate the harmonic distortion of the DN and to support the voltage and frequency of the DN. In addition, this project proposes a profit/energy optimization technique that will be included in the GSC controller in order to maximize the prosumer's profit under a variable electricity pricing environment. The aforementioned ancillary functionalities will enhance the value of PVs and enable an even wider adoption of PV systems by allowing new services to be promoted in the electricity market (e.g., support for ancillary services, increased market revenues and sustainability of the PV projects without government incentives). Through the new ancillary services of the proposed GSC of PV systems, the power quality and the stability of the DN can be significantly enhanced, the power losses of the DN will be minimized and the electricity price will be reduced. The clear advantages of the proposed operational approaches will benefit the distribution system operator (DSO) and the whole power system, the electricity consumer and prosumer, the environment, and can potentially benefit the PV industry and the consortium.

Regarding the Technology Readiness Level (TRL) of the project, the consortium will start from TRL-2, since the technology concepts of the several new operational approaches of the proposed GSC have already been formulated by the partners. By the project completion, the consortium will reach TRL-7 since the new operational functionalities of the proposed GSC will be experimentally validated and demonstrated as a prototype system. Additionally, this project aims to advance several crucial units/methodologies in the controller of the GSCs, which will be experimentally validated and by the end of the project will replace the corresponding methodologies of the existing GSCs.

Advancing all the crucial units of the GSC controller (e.g., synchronization method, current controller, PQ controller) and developing several new operational functionalities for the GSC are the main scientific and technical challenges of the project. The successful completion of the technical goals and challenges of the project is guaranteed by the expertise of academic partners in controller design of GSCs for PV systems, reliability of power electronic converters and optimization techniques. The performance improvement and the novel operational functionalities of the GSC can lead to potential economic benefits, especially by the new ancillary services enabled by the proposed GSC. Thus, the advantages of the new GSC in combination with the experience of the industrial partner (QE) on energy market investments will enable the project to meet its commercial challenges and achieve the commercial exploitation of the developed converters.

In the following, each work package (WP) of the project and milestones (MS) are shown in Fig. 4.1, and the status is described in terms of goals and achievements.

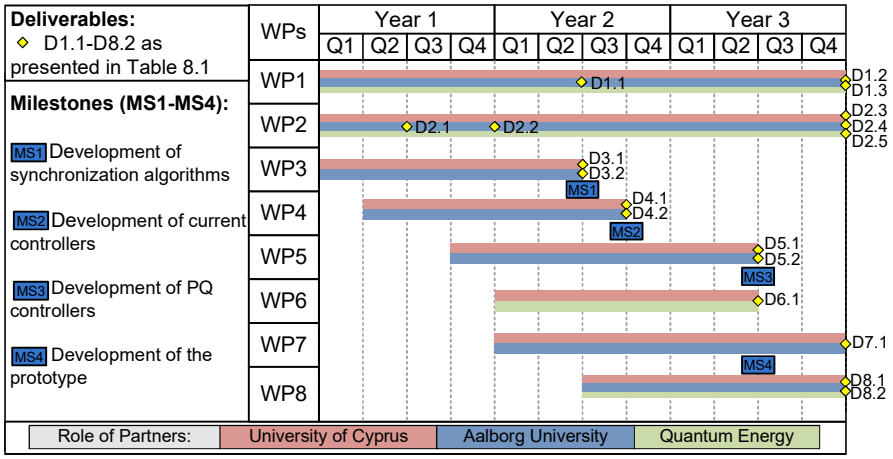

Fig. 4.1. Time schedule of each WP and the completion time of each milestone and deliverable.

WP1: Project Management

The objectives of this WP are the smooth and timely execution of the research work, the overall coordination of the project and the maintenance of an appropriate management structure throughout the project to ensure the success of the project. UCY (Project Coordinator) will have the major responsibility in this WP, but all partners will contribute. All partners are experienced in project management as evidenced by the large number of relevant research projects coordinated.

WP status: OK

Status of deliverables and milestones:

D1.1 Midterm report and financial report (UCY) - **Done**

D1.2 Final report and financial report (UCY) - **AAU has done; TBD by March 2018 by UCY**

D1.3 Minutes of the Consortium's exchange of visits (UCY) - **TBD by March 2018 by UCY**

WP2: Dissemination and Exploitation of Results

This WP will be responsible for the proper dissemination and exploitation of the results in the forms of web site publicity, publications in high quality scientific journals, seminars/tutorials, and conference presentations. An exploitation plan for the results of the project will be developed based on market assessment and the technological outcomes. Appropriate intellectual rights protection (e.g., patenting) will be taken. The dissemination of the results will be under the responsibility of all the partners and the exploitation of the project results will benefit the whole consortium. Public awareness campaigns will be undertaken throughout the project and one project workshop will take place in each country. SOLAR-ERA.NET will be explicitly acknowledged in all dissemination and exploitation activities.

WP status: The project has been well and widely disseminated at international conferences and top-tier journals. In total, the project has achieved **more than 40 publications**. **A special session** focusing on active power control for PV systems was organized at an international conference. The project has also **initiated an industrial project**, which is currently running at Department of Energy Technology, Aalborg University.

Status of deliverables and milestones:

D2.1 Link for the project web site and YouTube channel (UCY) - **Done**

D2.2 Posters/Info-graphics displayed at Host and Partner Organizations (UCY) - **Done**

D2.3 Publications in scientific journals (at least four) (AAU) - **Done**

D2.4 Presentations/posters presented to international conferences (at least four) (AAU) - **Done**

D2.5 News articles and project workshops (UCY) – 80%. One more workshop will be held at the University of Cyprus in March 2018. The project will then be closed at UCY as well.

WP3: Advanced Synchronization Methods

This WP focuses on developing new, fast and robust synchronization methods for single- and three-phase PV systems. The proper synchronization will enable the appropriate grid-connection of PV systems under any grid conditions and will increase the power quality of PV systems. The proposed synchronization methods will be of high accuracy and fast response in order to enhance the performance of the GSC. Furthermore, the synchronization algorithm will require limited processing time to enable the real-time operation of the PV system. Especially under low-voltage grid conditions, a fast synchronization can enable the required Fault Ride Through (FRT) operation of the GSC to provide proper support to the grid. The accuracy under harmonic distorted voltage is a critical aspect since unwanted oscillations on the synchronization signals can introduce serious problems and affect the power quality of the PV system. The proposed synchronization methods will be based on PLL and/or FLL algorithms designed in multiple synchronous reference frames (SRFs). The multiple SRFs will enable the dynamic decoupling of voltage sequences/harmonics through innovative cross-feedback networks in order to achieve a robust and accurate (better power quality) estimation of each voltage component without affecting the dynamic response (proper FRT) of the synchronization. This WP results are very important, since the synchronization can affect the response of the current controller (WP4) and the PQ controller (WP5) and hence the entire GSC (WP7). The expertise of UCY and AAU on synchronization methods will ensure the successful completion of the WP.

WP status: In this WP, several synchronization methods have been proposed and developed. Those enable a proper, accurate, fast, and robust synchronization of single-phase and three-phase PV systems. This is beneficial to PV integration in terms of FRT, harmonic compensation, current control and PQ control. The developed synchronization techniques are detailed in Section 5.

Status of deliverables and milestones:

D3.1 Report on the developed advanced synchronization methods (UCY) - **Done**

D3.2 Simulink models and/or executable C files for the new synchronization methods (UCY) - **Done**

MS1 Development of synchronization algorithms – **OK**

WP4: Design of Enhanced Current Controllers

One of the main goals of this project is the utilization of the GSC of PV systems to symmetrize the load and increase the quality of the prosumer. This aim will be achieved by the development of advanced current controllers with enhanced capabilities. Therefore, the main objective of this WP is to design new current controllers with the ability of controlling an accurate injection of positive, negative (in case of three-phase GSC) and harmonic currents under normal or abnormal voltage conditions. The advanced single- and three-phase current controllers will enable the use of PV systems and/or ESS for symmetrizing the load (on the three phases) and for enhancing the grid power quality by compensating the harmonics of the prosumer as a whole. Additional functionalities of the accurate operation of the proposed current controller under abnormal voltage conditions (unbalanced low voltage faults and/or harmonic distorted voltage) will allow more optimal operations of PV systems and ESS under any possible grid conditions. The current controllers proposed in this WP will be designed in multiple SRF with PI controllers or using cascading PR controllers or using repetitive control techniques to enable the injection currents to fast and accurately track the reference currents. AAU and UCY have proven through their work that they are

capable of designing and implementing such advanced controllers and so they can guarantee the success of this WP.

WP status: In grid-connected PV systems, one concern is on the power quality of the injected current. It is affected not only by the control of the GSC but also the grid conditions (e.g., faulty modes and background distortions). In this WP, **periodic controllers** (i.e., repetitive controllers and proportional resonant controllers) were adopted to enhance the power quality of currents injected by PV systems. The developed current controllers offer precise current control of GSC systems under different conditions (e.g., FRT, background harmonics, and grid frequency variations). Furthermore, **strategies to accurately inject positive- and negative-sequence components** were also developed for three-phase GSC systems.

Status of deliverables and milestones:

D4.1 Report with new enhanced current controllers (AAU) - **Done**

D4.2 Simulink models and/or executable C files for the new current controllers (AAU) – **Done**

MS2 Development of current controllers - **OK**

WP5: Development of PQ Controllers

This WP will focus on a higher-level control of the GSC, which will allow the proper operation of the PV systems and ESS under any possible mode. This controller can be a PQ controller enhanced with some additional functionalities (a different PQ controller is required for single- and three-phase PV system). This controller will be able to determine the direction of energy flow on the GSC, to satisfy a robust and efficient Maximum Power Point Tracking (MPPT) operation of the PV panels, the proper grid voltage (reactive power) support, and the FRT operation of the PV system. Additionally, the PQ controller will be responsible for the proper generation of the reference currents to enable the innovative operational approach for symmetrizing the three-phase load of the prosumer and additionally eliminating the harmonics of the prosumer to increase the quality and efficiency of DN. Therefore, the proposed flexible GSC will enable the prosumer to be seen from the grid as a symmetric and harmonic-free load, a fact that will benefit all the stakeholders. The development of such PQ controllers with advanced functionalities will be achieved by the collaboration and the high expertise of UCY and AAU.

WP status: A general PQ control strategy has been developed in this WP according to the *Instantaneous Power Theory*. For single-phase GSC systems, an Orthogonal Signal Generator is required when applying the PQ controllers; for three-phase GSC systems, it is intuitive to adopt the PQ controllers. The developed PQ controllers enable multifunctional GSC systems.

Status of deliverables and milestones:

D5.1 Report on the developed advanced PQ controller for single- and three-phase GSC (AAU) - **Done**

D5.2 Simulink models and/or executable C files for the developed PQ controller (AAU) - **Done**

MS3 Development of PQ controllers - **OK**

WP6: Profit/Energy Scheduling Algorithm

An optimal scheduling algorithm is a useful feature to be integrated in the bi-directional converter, especially when the prosumers are connected to a network with a dynamic electricity-pricing environment and when an ESS is available on the DC link of the GSC. The scheduling algorithm will be run by the controller of the GSC. Currently, there are market solutions (as separate tools), mainly for the energy management of home systems with PV and storage. However, they typically use a basic management scheme with prioritization and with the objective of maximizing self-consumption

within the system. The proposed algorithm aims to maximize the profit of the prosumers by managing the injection/absorption of energy from the GSC.

The new algorithm is based on advanced stochastic optimization, such as stochastic linear programming, which explicitly takes into account the uncertainty of some input variables such as: weather, power output prediction data and electricity prices. Therefore, the model works with confidence intervals instead of single average points in order to determine the optimal set points. The outcomes of the scheduling algorithm will feed in the PQ controller (WP5) in order to regulate the operation of the bidirectional GSC. The collaboration of UCY with QE (electricity market knowledge) will ensure a successful completion of this WP.

WP status: Due to the fact that QE was not funded in this project, the work in this WP is delayed. UCY has contacted with another department at the University of Cyprus. This WP will then be done by March 2018.

Status of deliverables and milestones:

D6.1 Report for the developed Profit/Energy Scheduling Algorithm (UCY) - 50%.

WP7: Prototyping Development

The proposed synchronization methods, current control techniques, PQ controllers and scheduling algorithm will be implemented in the controller of the GSC to develop experimental prototypes of the proposed GSC. The single- and three-phase power electronic converters for the prototype setups are already available in the laboratories of partners and the advanced controller of the GSC will be implemented using an available Texas Instrument TMS320F28335 digital signal controller or a dSPACE DS1103 digital signal processor board. The experimental setup will consist of the prototype GSC and several unbalanced and harmonic loads acting as the prosumer loads to verify the proper operation of the developed GSC and its controllers. The proposed control for the GSC will enable the harmonic and unbalanced current injection from the PV system to compensate and/or symmetrize the prosumer currents. The proposed next-generation GSC will be tested under several grid conditions and under several (harmonic and unbalanced) loading conditions. Furthermore, several ancillary services provided by the advanced GSC will be experimentally validated. UCY and AAU will collaborate for the prototype development and the experimental validation of the project results and the available laboratories in the infrastructure of the consortium will be utilized in order to complete this WP.

WP status: A prototype of the single-phase GSC and three-phase GSC PV system have been developed at Aalborg University and University of Cyprus, respectively. Those prototypes have been used to test/verify the developed control strategies. Section 5 will give a detailed description of the developed prototypes.

Status of deliverables and milestones:

D7.1 Technical report for the prototype and the experimental results of the project (UCY) - **Done**

MS4 Development of the prototype - **OK**

WP8: Reliability and Cost Benefit Analysis

The proposed unbalanced and harmonic current injection from the GSC requires in-depth analysis, e.g., examining the possible impacts on the reliability of the power converters, impact on the power system operation, etc. The reliability and cost benefit analysis are impacted by the time horizon within the prototyping, commercialization and lifetime of the proposed GSC. The following tasks will be performed during this WP:

- Thermal loading analysis for the proposed GSC, including the capacitor life study.
- Development of a lifetime estimation method to verify if the proposed operation mode can affect the reliability of the GSC.
- Cost Benefit Analysis for the GSC, where GSC-enabled services will be treated as exogenous input for evaluation of the benefits (direct and indirect benefits), and the estimation/calculation methods for both benefits' and costs' quantization matrices will be derived from literature review of similar projects, where appropriate, or through surveys.
- Development of a business plan for the new ancillary services provided by the proposed GSC (e.g., load balancing, power quality enhancement, etc.).

AAU will perform the reliability analysis of the proposed GSC and the cost benefit analysis will be carried out by the collaboration of UCY and QE.
WP status: Reliability analysis of the GSC with advanced control strategies has been done by AAU. Due to the absence of QE, the cost-benefit analysis is delayed. This is expected to be finalized by March 2018 by UCY.

Status of deliverables and milestones:

D8.1 Technical report for the reliability analysis of the proposed GSC (AAU) - **Done**

D8.2 Report for the cost benefit analysis and business plan of the new GSC (QE) - **TBD by March 2018 by UCY**.

5. Project Outcomes

The main technical results of the project are the developed advanced control strategies for improving gird-integration of PV system with several aspects as following.

- *Prototype Development*

In order to verify the proposed advanced control strategy, a prototype of single- and three-phase grid-connected PV system has been developed at Aalborg University and University of Cyprus, respectively.

At Aalborg University, the prototype of single-phase PV system was developed according to the system configuration and control structure in Fig. 5.1. A photo of the setup is shown in Fig. 5.2. Here, a two-stage PV system consisting of a boost dc-dc converter and a full-bridge dc-ac inverter (PV inverter) is employed as an interface between the PV arrays and the ac grid. In this control scheme, the boost converter is responsible for power extraction from the PV arrays. Typically, the Maximum Power Point Tracking (MPPT) algorithm, e.g., Perturb and Observe (P&O) MPPT, is implemented in the boost converter to determine the operating PV voltage v_{pv}. Then, the PV inverter (full-bridge inverter) delivers the extracted power to the ac grid by regulating the dc-link voltage v_{dc} to be constant. In order to do so, the current controller is acting to regulate the grid current i_g according to a reference given by the dc-link voltage controller or a PQ controller. Notably, a Phased-Locked Loop (PLL) is also implemented to extract the phase angle of the grid in order to determine the reference grid current.

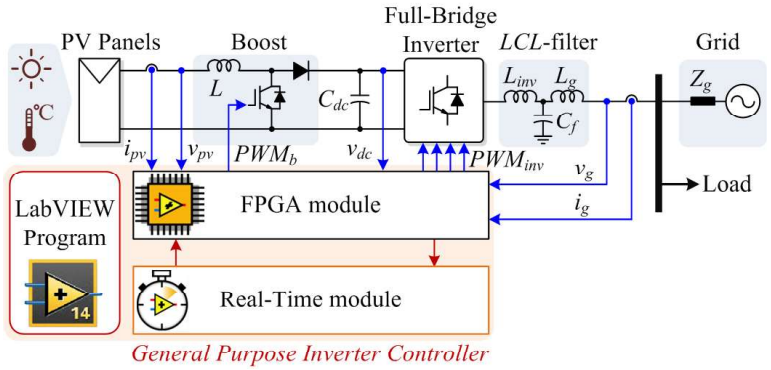

Fig. 5.1. System configuration and control structure of a single-phase grid-connected PV system.

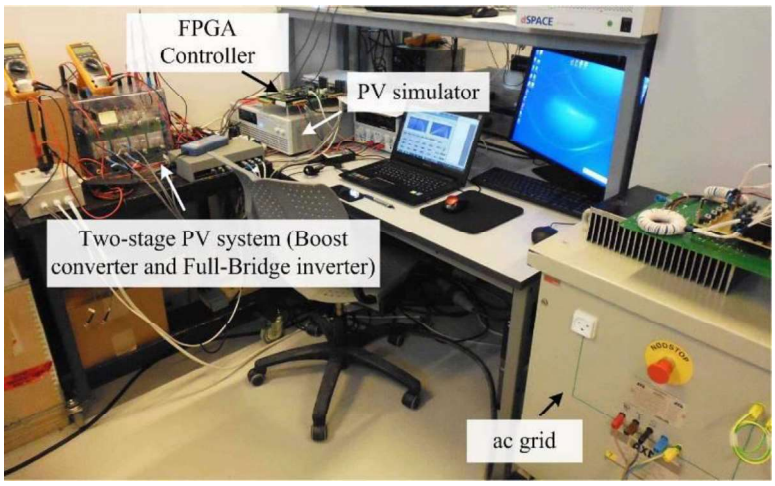

Fig. 5.2. Photo of the single-phase experimental setup.

The experimental setup of the three-phase grid-connected PV systems has been realized at University of Cyprus. A Delta Elektronika Power Supply (SM 600-10) operates as a DC source to emulate the energy produced from the RES and a Danfoss FC302 2.2 kW inverter acts as the GSC. A California Instruments 4500LX programmable AC source in combination with a parallel connected 3 kW load is used to emulate the power grid. The control has been designed using a dSPACE DS1103 DSP board in combination with the dSPACE Control Desk and MATLAB/Simulink Real Time Workshop. The sampling rate and the switching frequency of the designed GSC controller have been set to 7.5 kHz. The schematic of the experimental setup is presented in Fig. 5.3 and a photo of the setup is shown in Fig. 5.4.

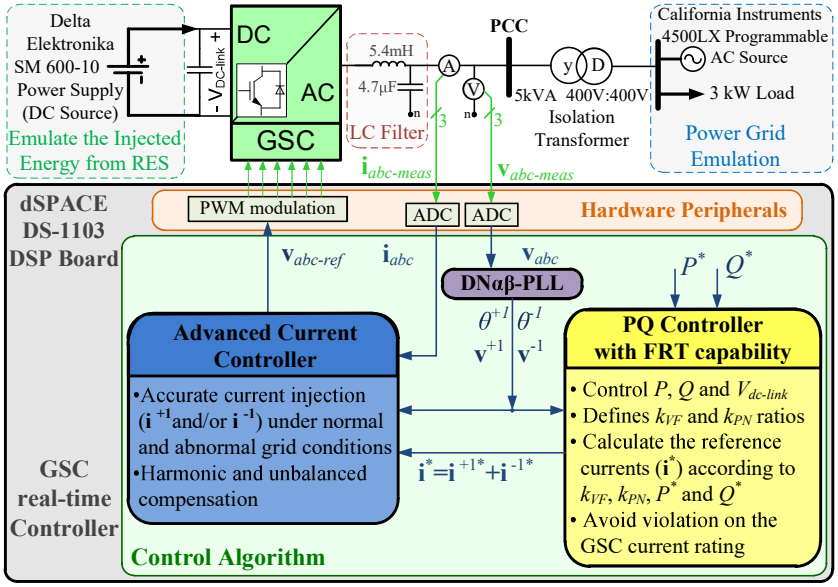

Fig. 5.3. Schematic of the experimental setup and the diagram of the advanced controller for the grid-connected RES.

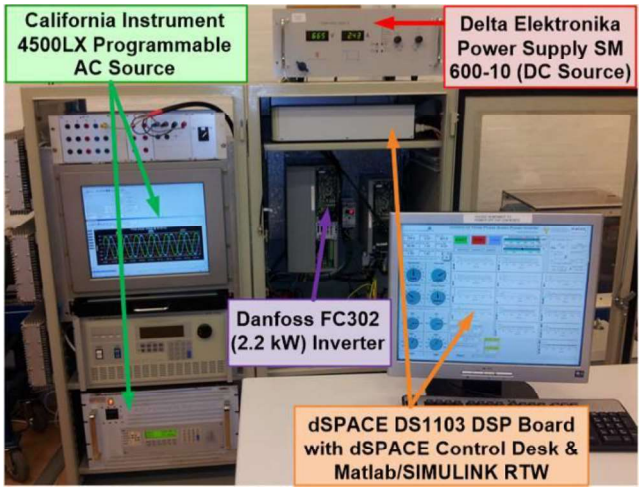

Fig. 5.4. Photo of the experimental setup.

➢ *Development of synchronization algorithms*

The synchronization method is the cornerstone of the GSC, since it is responsible for the injection of the produced PV power into the grid in a synchronized way. In this project, two advanced synchronization methods have been proposed for three-phase and single-phase GSCs, respectively, and also a conventional synchronization for single-phase GSCs has been enhanced. The description and results of the proposed method are discussed in the following.

(1) A three-phase synchronization method, named "DNαβ-PLL".

The new decoupling network allows an accurate detection of each voltage vector component $\mathbf{v}^n$, by dynamically cancelling-out the oscillations that are created due to the coupling effect between the voltage components. The block diagram of the proposed decoupling network (DNαβ) is shown in Fig. 5.5. The proposed DNαβ enables a proper decoupling between the existing voltage vector components and therefore can dynamically and accurately estimate the value of each voltage vector component ($\mathbf{v}_{\alpha\beta}{}^{n*}$ and $\mathbf{v}_{dq}{}^{n*n}$). The proposed PLL can be implemented by using the estimation of the pure positive sequence voltage component ($\mathbf{v}_{\alpha\beta}{}^{+1*}$), estimated by the DNαβ, as an input to the conventional αβ-PLL algorithm.

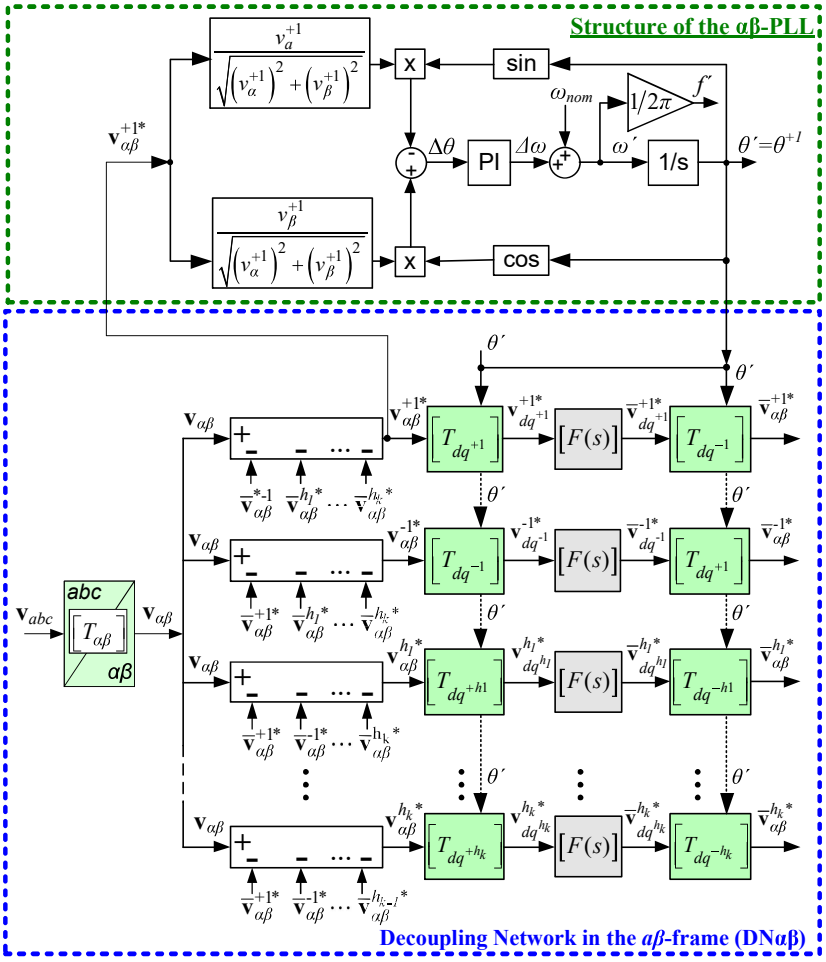

Fig. 5.5. The structure of the proposed DNαβ-PLL.

A simulation case study presented in Fig. 5.6 provides a comparison between the response of the proposed DNαβ-PLL, the dαβ-PLL, and the ddsrf-PLL. It is obvious that the proposed PLL achieves an accurate response under highly distorted grid voltage, where the Harmonic Conditions (HC) 1-3 are explained in TABLE 5.1. The ddsrf-PLL and dαβ-PLL present similar dynamic performance, but their accuracy is affected by the harmonic distortion. Moreover, Fig. 5.6 demonstrates that the accurate response of the new PLL is achieved without affecting the dynamic performance of the synchronization since the DNαβ-PLL presents a similar dynamic response with the dαβ-PLL and ddsrf-PLL under several faults. The proper and robust performance of the new PLL is verified under an unbalanced low-voltage grid fault (Type D with a voltage sag (*d*) of 37%), a 15° phase shifting fault and a frequency step of -0.2 Hz. The appropriate performance of the proposed PLL is also experimentally validated under harmonic distorted voltage and unbalanced grid fault as shown in Fig. 5.7. The experimental results prove the accurate and dynamic response of the new PLL under harmonic distorted voltage and grid disturbances.

The results, presented in Fig. 5.6 and Fig. 5.7, show that the proposed PLL achieves an accurate synchronization and the oscillation-free estimation of the synchronization signals (θ' *and* $\mathbf{v}_{dq}{}^{+1*\,+1}$). The synchronization signals are used from the PQ controller to generate the reference currents. Additionally, the operation of the current controller is based on an accurate estimation of the synchronization signals so it is expected that the accurate synchronization is directly affecting the GSC control and as a consequence the performance of the RES. An experimental investigation is presented here to prove how the accurate synchronization through the proposed PLL can enhance the power quality of the RES.

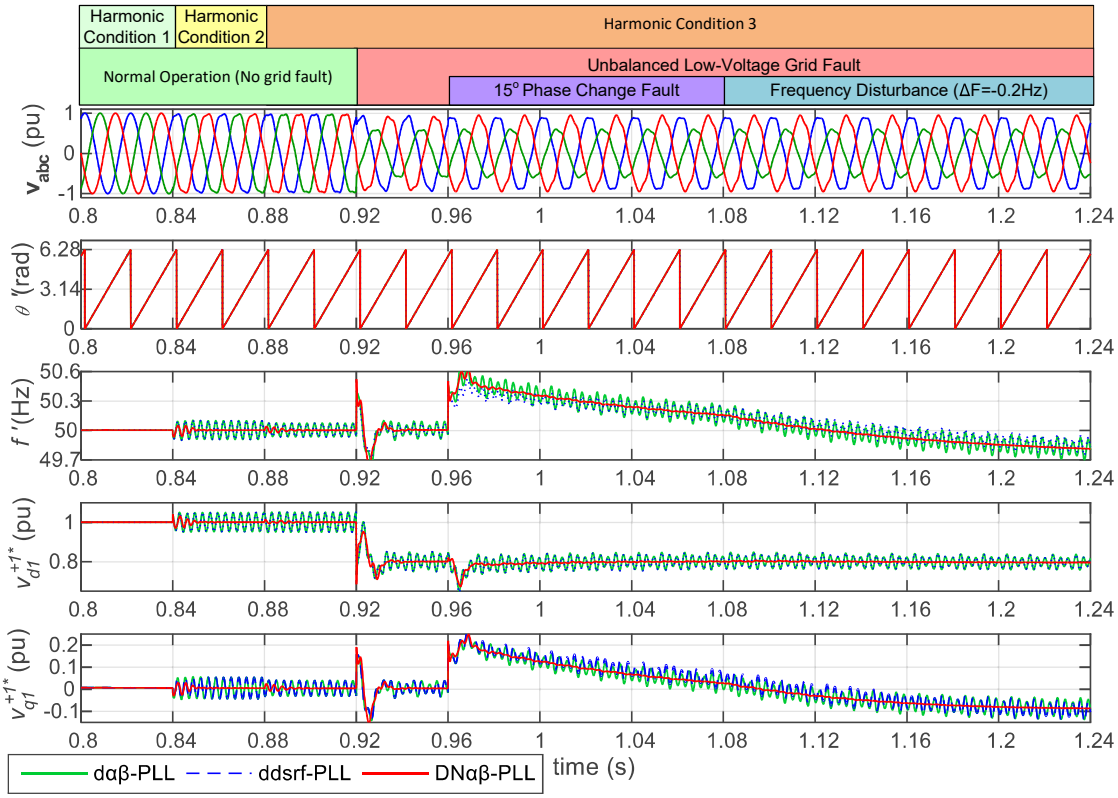

Fig. 5.6. Simulation results comparing the PLL response of the new DNαβ-PLL, the ddsrf-PLL, and the dαβ-PLL under several abnormal grid conditions.

TABLE 5.1: Summary of the results of Fig. 5.6.

Grid Conditions	MAF-PLL	mod. MRF-PLL	DNαβ-PLL
Harm. Distort. & f=50 Hz	√	√	√
Harm. Distort. & **a Voltage Sag occurs**	slow	slow	fast
• Settling Time (ϑ_{error}<0.1°)	99.7 ms	89 ms	57 ms
• Peak-Peak Phase error at 50 Hz	0 °	0 °	0 °
• Peak-Peak Freq. error at 50 Hz	0 Hz	0Hz	0Hz
Harm. Dist./Unbalanced & **Freq. Step**			Fast & accurate
• Settling Time (f_{error}<0.01 Hz)	130 ms	74 ms	70 ms
• Peak-Peak Phase error at 49.75 Hz	0.19 °	0.05 °	0 °
• Peak-Peak Freq. error at 49.75 Hz	0.041 Hz	0.012 Hz	0 Hz

The steady state performance of the grid-connected RES based on experimental results is presented in Fig. 5.8 under a highly harmonic distorted grid voltage (with harmonic condition 2 (HC-2) as explained in TABLE 5.2. Fig. 5.8(a) demonstrates the RES performance when the proposed DNαβ-PLL is used for the synchronization. It is shown that the new PLL estimates accurately the synchronization signals and therefore the reference currents are generated without any oscillations due to the harmonic distortion. Therefore, the RES achieves to inject high quality currents with a total harmonic distortion (THDi) of 2.6%. On the other hand, Fig. 5.8(b) presents the RES operation when the RES uses the dαβ-PLL for the synchronization. The inaccuracies of the dαβ-PLL, caused by the harmonic distortion, raise oscillations on the synchronization signals and therefore, the generated reference currents and the operation of the current controller are affected. Consequently, the RES with a non-robust synchronization against harmonics presents a low quality current injection with a THDi of 5.6% (outside of the grid code limits) under harmonic distorted grid voltage. This experimental case study proves that the accurate synchronization is a key aspect for the power quality of the RES.

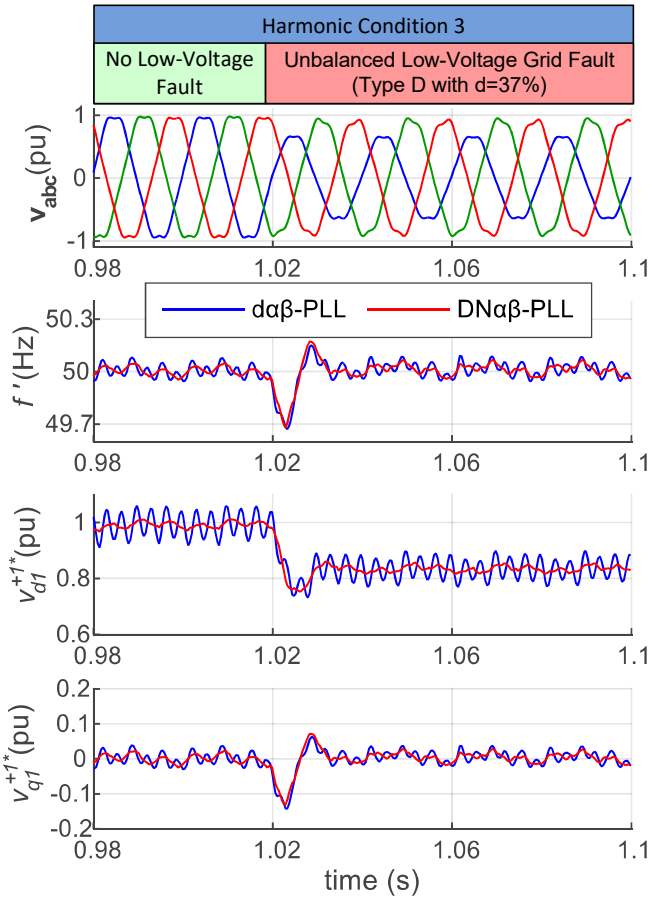

Fig. 5.7. Experimental results presenting the accurate response of the new DNαβ-PLL under harmonic distorted and unbalanced grid voltage.

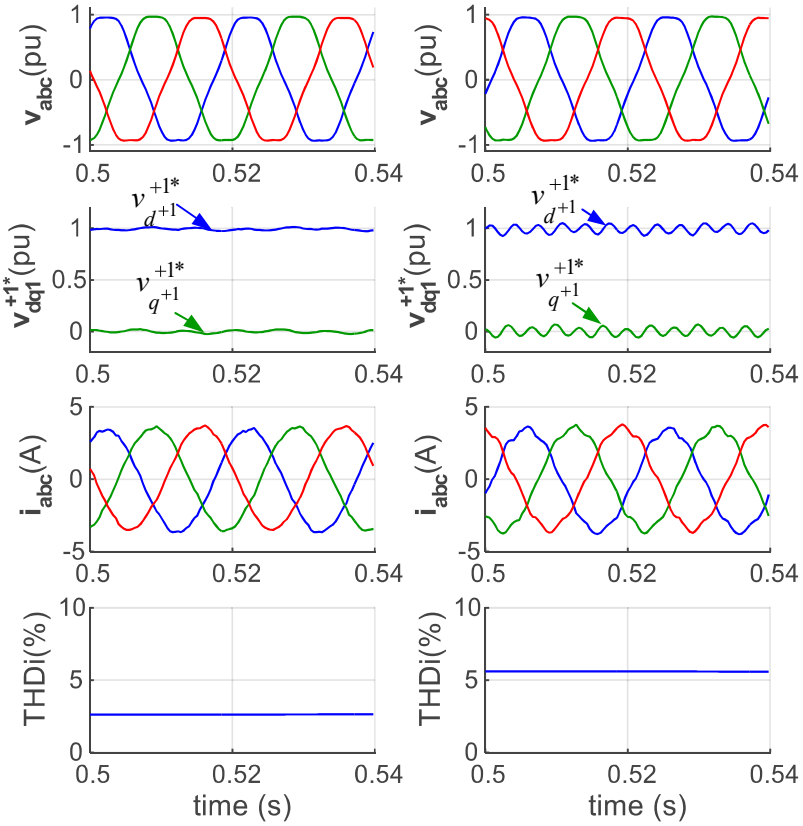

(α) RES response (with DNαβ-PLL) (b) RES response (with dαβ-PLL)

Fig. 5.8. Experimental results for the performance of the RES under harmonic distorted voltage, when using (a) the proposed DNαβ-PLL and (b) the dαβ-PLL for the synchronization of the GSC.

TABLE 5.2: THE IMPACT OF THE ACCURATE SYNCHRONIZATION THROUGH THE PROPOSED SYNCHRONIZATION ON THE POWER QUALITY OF RES.

Grid Operating Conditions			Synchronization Method	
			dαβ-PLL	DNαβ-PLL
Low Voltage Fault	**Voltage Harmonic Distortion**	**Freq (Hz)**	**THD(%) of the injected currents**	
No Fault	HC-1	50	2.45	2.45
No Fault	HC-2	50	5.60	2.60
ULVF-1	HC-2	50	6.50	4.00
ULVF-1	HC-2	49.5	6.65	4.20
No Fault	HC-3	50	5.10	2.90
ULVF-1	HC-3	50	6.05	4.40
ULVF-1	HC-3	49.5	6.30	4.55

Index:

- ULVF-1: Type D Unbalanced Low Voltage Fault with d=37%
- HC-1: Harmonic Cond. 1 (High-frequency harmonics (HFH)=0.1%)
- HC-2: Harmonic Cond. 2 (THD_V=5% with $|V_5|$=4.9%, HFH=0.1%)
- HC-3: Harmonic Cond. 3 (THD_V=4.57% with $|V_5|$=4%,$|V_7|$=2%, HFH=0.1%)
- HC-4: Harmonic Cond. 4 ($|V_5|$=6%, $|V_7|$=5%, $|V_{11}|$=3.5%, $|V_{13}|$=3%, $|V_{17}|$=2%, $|V_{19}|$=1.5%, $|V_{23}|$=1.5%, $|V_{25}|$=1.5%, $|V_{19}|$=1.5%, HFH=0.1%)

The dynamic response of the GSC is a critical aspect, especially under low-voltage grid faults, where the RES should immediately support the faulty grid. Thus, it is important to prove that the proposed DNαβ- PLL can enable the proper dynamic FRT performance of the RES when a fault occurs in order to meet the grid regulations. The experimental case study presented in Fig. 5.9 shows the RES performance when operating under harmonic distorted voltage (harmonic condition 2 as shown in TABLE 5.2) and an unbalanced low-voltage grid fault occurs. The RES is operating in the 80% of the GSC ratings before the occurrence of the low-voltage fault. When the fault occurs, the proposed DNαβ-PLL ensures the accurate and fast estimation of the synchronization signals as shown in Fig. 5.9. The proper synchronization enables the fast and adequate FRT operation of the PQ control algorithm to ensure the full positive current injection (k_{PN}= 1), the support of the grid with k_{VF}= 0, and the limitation of the current injection within the converter limits.

(2) A single-phase synchronization method, named “Frequency adaptive MHDC-PLL”

In this part, a novel single-phase synchronization method, which can achieve an accurate and fast synchronization performance under several grid voltage disturbances and also when the distribution grid contains both low- and high-order harmonics, is proposed. The frequency adaptive MHDC-PLL is a state-of-the-art synchronization technique and can be ideally used by the single-phase GSC to inject the power produced by residential PVs into the grid. The frequency adaptive MHDC-PLL is based on (a) a frequency adaptive QSG which is accurate under any frequency conditions and can eliminate the effect of high order harmonics, (b) an improved Multi-Harmonic Decoupling Cell that ensures a fast decoupling of the fundamental voltage component with a reasonable required processing time, and (c) a conventional dq-PLL algorithm.

The proposed frequency adaptive MHDC-PLL is developed based on the adaptive QSG, as it is shown in Fig. 5.10. The adaptive QSG is based on the IPT method in order to filter out the high-order harmonics and then the proposed frequency adaptive T/4 delay unit is used to generate the voltage vector $\mathbf{v}_{\alpha\beta}$. The proposed frequency adaptive method overcomes the inaccuracies under non-nominal frequencies caused by the initial QSG and thus, an accurate operation can be achieved under any grid frequency. Then, the $\mathbf{v}_{\alpha\beta}$ is fed to the proposed improved MHDC as shown in Fig. 5.10, in order to dynamically cancel out the effect of low-order harmonics.

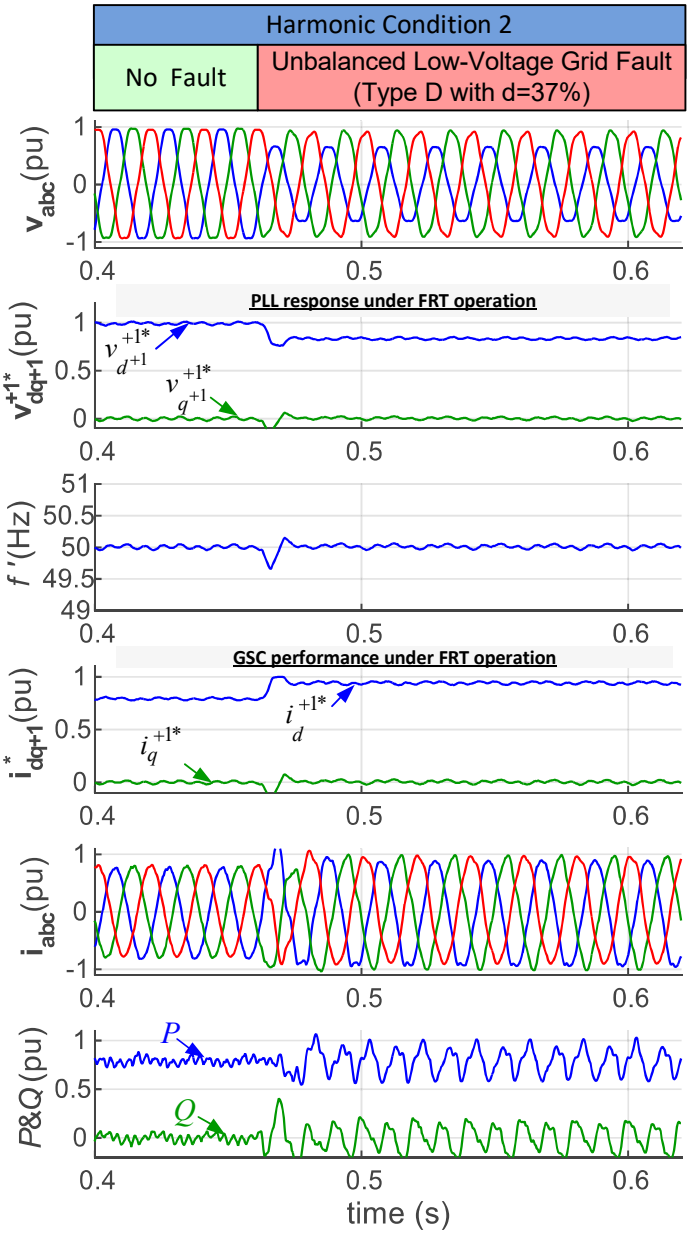

Fig. 5.9. The FRT performance of a grid-connected RES, when the new DNαβ-PLL is used for the synchronization, under unbalanced grid fault and harmonic distorted voltages.

The performance of the proposed frequency adaptive MHDC-PLL has been tested through simulation and experimental results in order to demonstrate the outstanding response of the new synchronization method. The results are presented in Fig. 5.11 which shows the synchronization response of the frequency adaptive MHDC-PLL and the initial MHDC-PLL under the worst-case harmonic distortion at 0.3 s, a 10° phase jump at 0.4 s, a 25% voltage sag at 0.5 s and -1.5 Hz frequency change at 0.6 s. The performance comparison between the two PLLs proves that the frequency adaptive implementation of the QSG enables the accurate synchronization under non-nominal frequencies (0.6<*t*<0.75 s). Therefore, the frequency adaptive MHDC-PLL not only requires a significantly less processing time. From Fig. 5.11, it is obvious that the new frequency adaptive MHDC-PLL presents a very accurate response (even under the worst-case harmonic distortion for t>0.3 s) and a very fast synchronization under any grid disturbance (e.g., phase jump, voltage sag, frequency change).

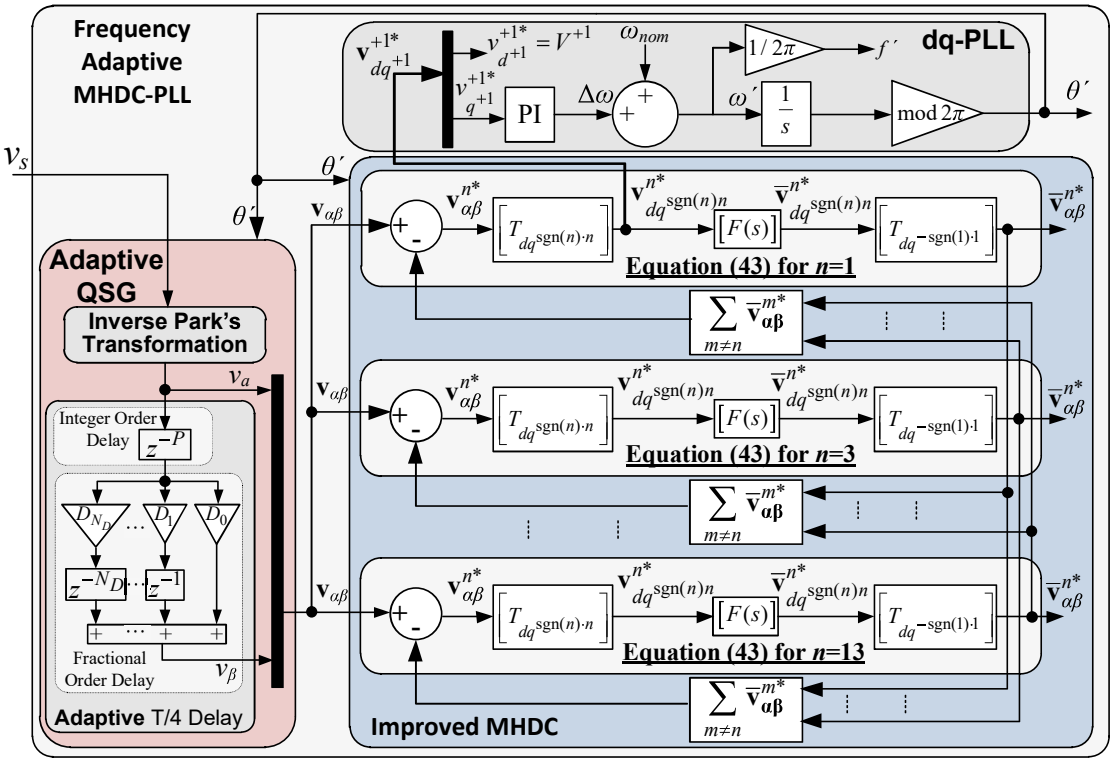

Fig. 5.10. The structure of the proposed frequency adaptive MHDC-PLL.

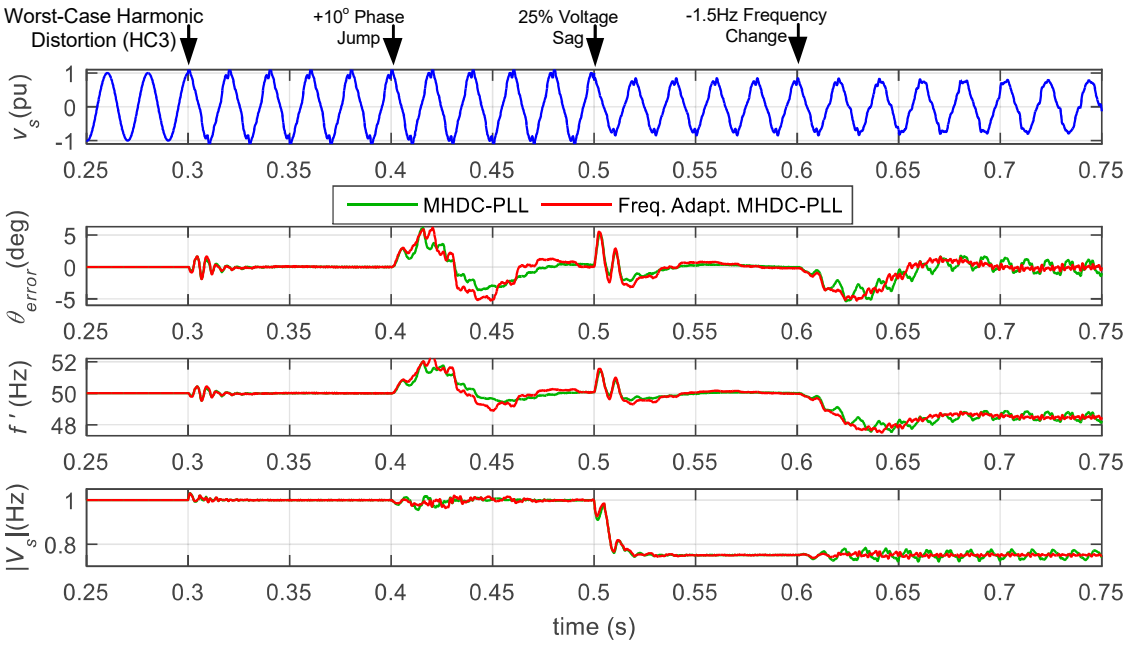

Fig. 5.11. Simulation results for the response of the frequency adaptive MHDC-PLL and the initial MHDC-PLL of [23] under harmonic distortion, phase jump, voltage sag and frequency change events.

The superior synchronization performance of the proposed frequency adaptive MHDC-PLL has also been experimentally verified as shown in Fig. 5.12. The experimental results of Fig. 5.12(a) demonstrate the response of the new synchronization method when the worst-case harmonic distortion occurs at the grid voltage. The experiments show that the proposed PLL can decouple the effect of harmonics within 10 ms. The initial voltage in Fig. 5.12(b)-(d) has harmonic distortion with the worst-case harmonics and then a grid disturbance is applied. According to Fig. 5.12(b), a fast and accurate synchronization is achieved under a 25% voltage sag, which can enable a proper FRT operation of the grid tied inverter. Fig. 5.12(c) demonstrates the operation of the new PLL under a 1 Hz frequency change. It is worth mentioning that the frequency adaptive MHDC-PLL presents a very accurate response under non-nominal frequencies due to the adaptive QSG. Finally, the fast and

accurate synchronization response under a 10° phase jump is demonstrated in Fig. 5.12(d). According to the experiments of Fig. 5.12, the proposed frequency adaptive MHDC-PLL can achieve a fast and accurate synchronization under any grid conditions. Such an advanced PLL based synchronization method can be an ideal solution for the synchronization of grid tied inverters.

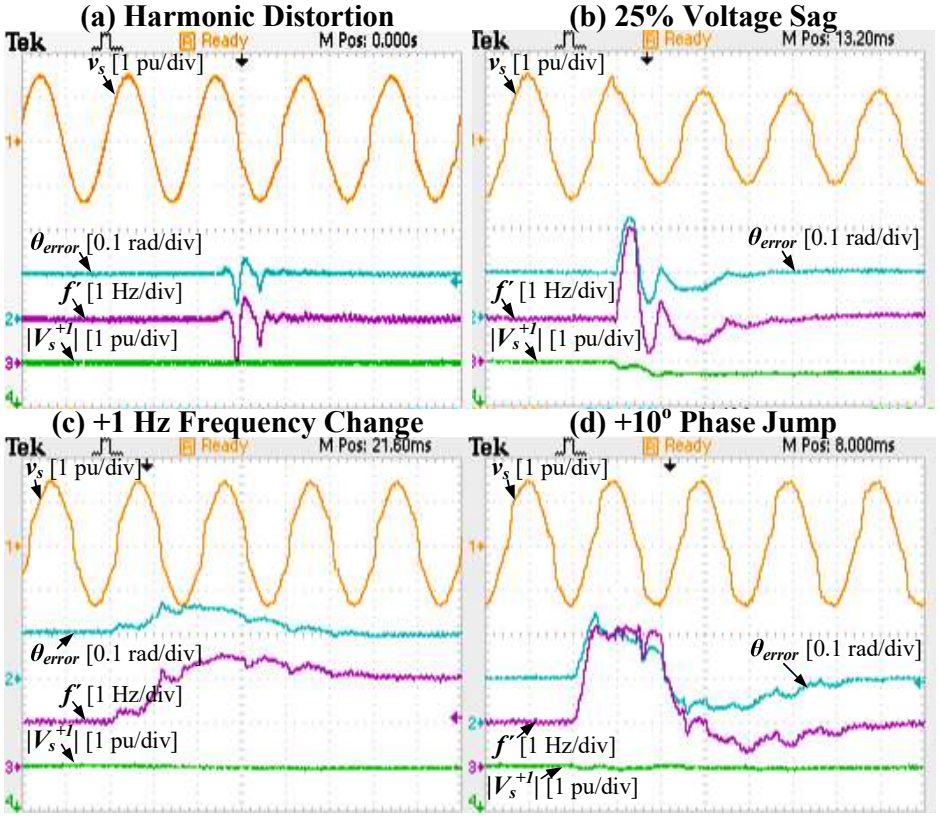

Fig. 5.12. Experimental results for the synchronization response of the frequency adaptive MHDC-PLL under: (a) a harmonic distorted voltage, (b) a 25% voltage sag, (c) a 1 Hz frequency change, and (d) a 10° phase jump. The time division of the results is 10 ms/div.

A simulation based investigation has been performed here to demonstrate the beneficial effect of a fast and accurate synchronization on the operation of the grid-tied inverter as shown in Fig. 5.13. During the FRT operation the injected active power is decreased to maintain the injected current within the inverter limits. Hence, the results of Fig. 5.13 demonstrate that the accurate and fast response of the frequency adaptive MHDC-PLL is particularly beneficial for the operation of the grid tied inverter, in terms of increasing the power quality and of enabling an appropriate dynamic and FRT operation of the inverter.

(3) Enhanced Single-phase T/4 Delay PLL

One of the single-phase PLL synchronization techniques—T/4 Delay PLL—is attractive due to its simplicity and easy to implement. However, the T/4 Delay PLL also suffers from harmonics and grid-frequency variations. Thus, the first attempt that has been made to improve the synchronization was to replace the conventional T/4 delay unit with a frequency adaptive scheme. The frequency adaptive scheme is the same as that used in the frequency adaptive MHDC-PLL (see Fig. 5.10). That is, the fractional number of delays is approximated using the *Lagrange Interpolation Polynomial* method. To tackle the impact of grid background distortions on the synchronization, a periodic signal filter, also known as a comb filter, has been adopted to filter out the harmonics. The structure of the enhanced single-phase T/4 Delay PLL is shown in Fig. 5.14.

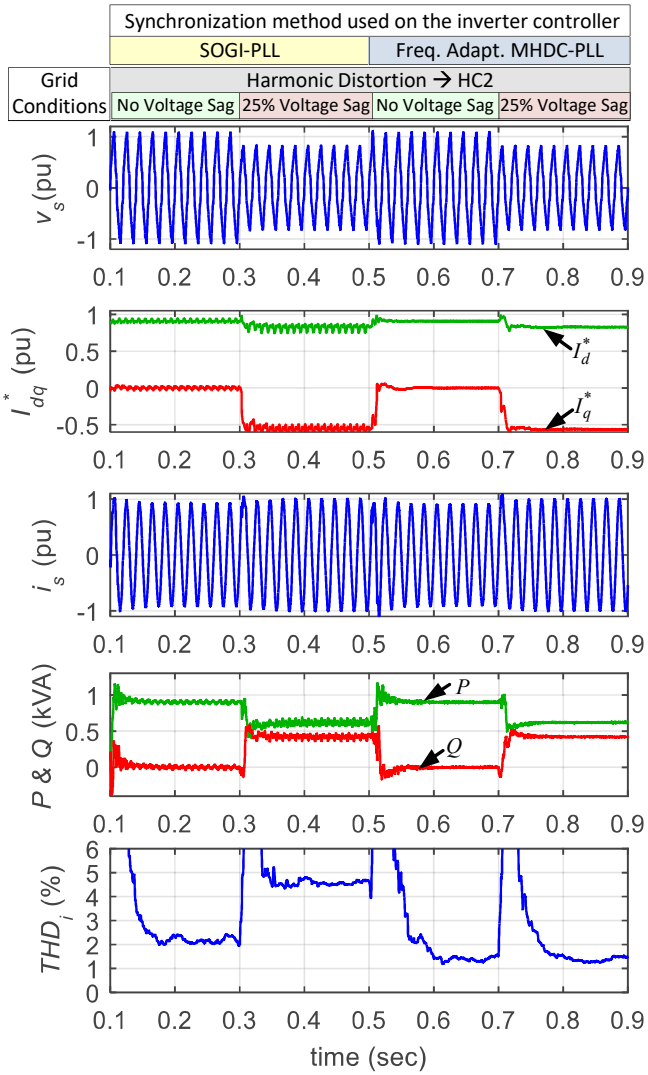

Fig. 5.13. Simulation results for the inverter operation when (a) a SOGI-PLL and (b) a frequency adaptive MHDC-PLL is used for the synchronization of the inverter under harmonic distorted voltage and a voltage sag event.

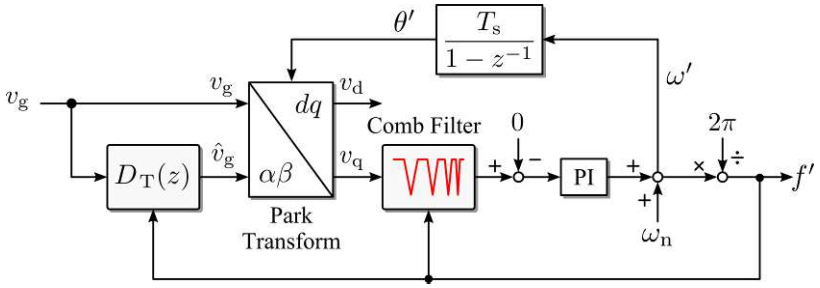

Fig. 5.14. Structure of the digital T/4 Delay PLL using the frequency adaptive T/4 Delay unit DT(z) and a frequency adaptive comb filter for single –phase systems, where the comb filter is used to filter out the even-order harmonics.

Experimental tests have been performed on the enhanced single-phase T/4 Delay PLL system. A comparison between the conventional T/4 Delay PLL and the enhanced one has also been done. The results are shown in Fig. 5.15. In the experiments, the grid voltage has harmonics (3rd-order: 2.2%, 5th-order: 1.7%, 7th-order: 0.4%, 9th-order: 1.4%, and 11th-order: 0.5%), leading to the total harmonic distortion of the grid voltage being 3.3%. Clearly, as seen in Fig. 5.15, the enhanced PLL with frequency-adaptive T/4 delay unit and the comb filter can improve the performance, which gives an almost harmonic-free estimated frequency.

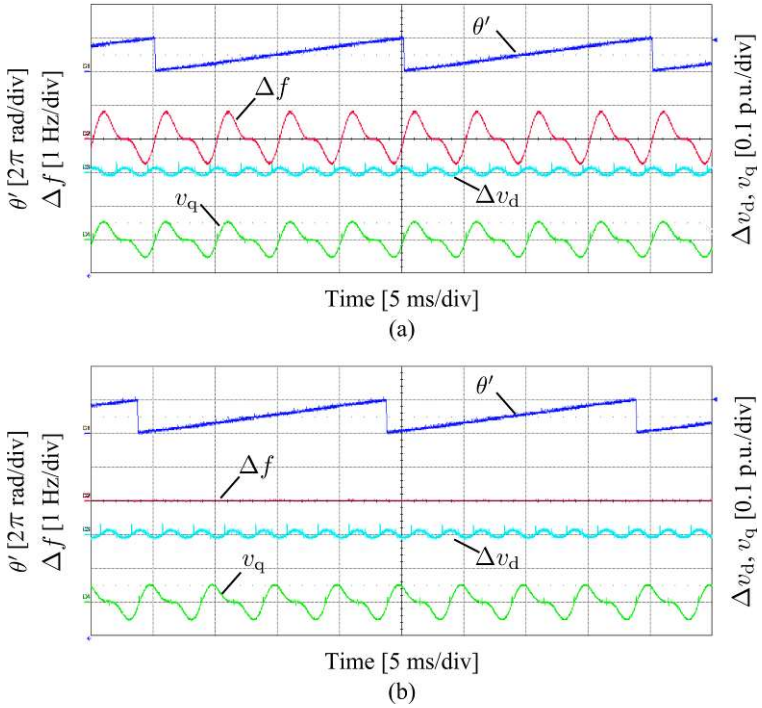

Fig. 5.15. Experimental results (the estimated frequency error Δf; the estimated d-axis voltage error $\Delta v_d = (v_d - 325)/325$) of the conventional T/4 Delay PLL system under low-order voltage distortions: (a) without and (b) with the frequency adaptive delay unit $D_T(z)$ and the comb filter.

The above outcomes mainly appear in:

[1] L. Hadjidemetriou, E. Kyriakides, and F. Blaabjerg, "A robust synchronization to enhance the power quality of renewable energy systems," *IEEE Trans. Ind. Electron.*, vol. 62, no. 8, pp. 4858-4868, Aug. 2015.

[2] L. Hadjidemetriou, E. Kyriakides, Y. Yang, and F. Blaabjerg, "A synchronization method for single-phase grid-tied inverters", *IEEE Trans. Power Electron.*, vol. 31, no. 3, pp. 2139-2149, Mar. 2016.

[3] L. Hadjidemetriou, Y. Yang, E. Kyriakides, and F. Blaabjerg, "A synchronization scheme for single-phase grid-tied inverters under harmonic distortions and grid disturbances," *IEEE Trans. Power Electron.*, vol. 32, no. 4, pp. 2784-2793, Apr. 2017.

[4] Y. Yang, K. Zhou and F. Blaabjerg, "Virtual unit delay for digital frequency adaptive T/4 delay phase-locked loop system," in *Proc. IEEE IPEMC-ECCE Asia*, Hefei, 2016, pp. 2910-2916.

[5] Y. Yang, Z. Xin, K. Zhou, and F. Blaabjerg, "Unified digital periodic signal filters for power converter systems," in *Proc. IFEEC 2017 - ECCE Asia*, Kaohsiung, 2017, pp. 286-291.

- *Development of Current Controllers*

The main objectives of WP4 are the design and development of enhanced current controllers for three-phase and single-phase Grid Side Converters (GSCs) of Photovoltaic (PV) systems. These objectives have been completely achieved and as a consequence, several new current control techniques have been design within the PV2GRID project. The main outcomes of the WP4 of the PV2GRID are summarized:

- High-performance current controllers based on repetitive control scheme for accurate control of the grid currents injected by PV systems considering the grid frequency variations.
- Method for proper generation of current references when using PV systems and/or ESS to compensate the grid harmonics.
- Enhanced current controller for harmonics of PV systems under different operation modes.
- Current controller based on decoupling network for on purpose positive and negative current injection.
- Advanced current controller with reduced complexity and improved performance under unbalanced conditions.

- Type B computationally efficient current controller for injection of both positive and negative current sequences.
- Extended type D current controller for on purpose injection of both positive and negative sequences and harmonic distorted currents.

In the following, the outcomes are selectively presented:

(1) High-performance current controllers based on repetitive control scheme for accurate control of the grid currents injected by PV systems.

The main objective of this task is to make the periodic current controllers to be frequency adaptive. Widely used examples for periodic current controllers are the Proportional Resonant (PR) current controller with parallel RESonant (RES) controller as shown in Fig. 5.16(a) and the PR current controller with parallel Repetitive Controller (RC) as shown in Fig. 5.16(b). The parallel RES or RC is mainly used as a harmonic compensation unit in order to achieve high quality current injection under voltage harmonic distortion.

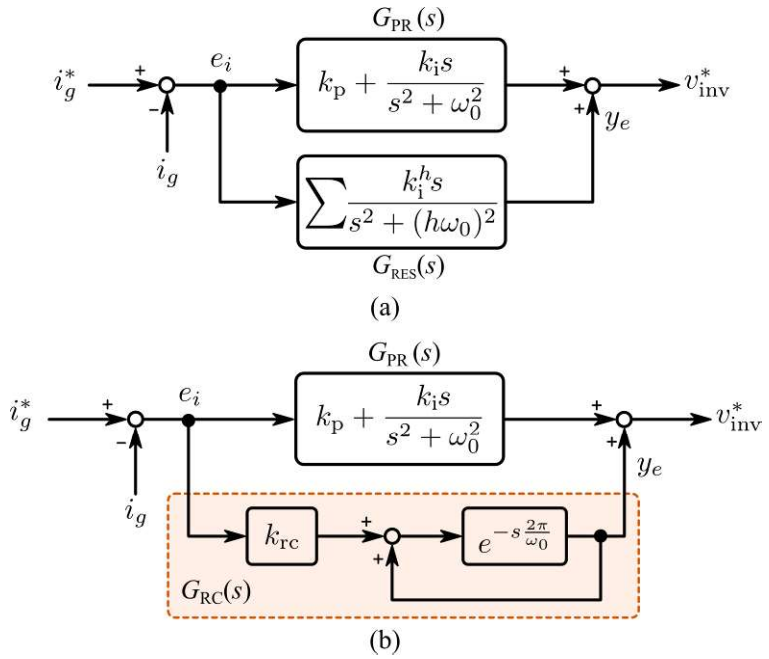

Fig. 5.16. PR current controller *G*PR (*s*) with (a) resonant harmonic controller G_{RES} (*s*) and (b) repetitive harmonic compensator G_{RC} (*s*).

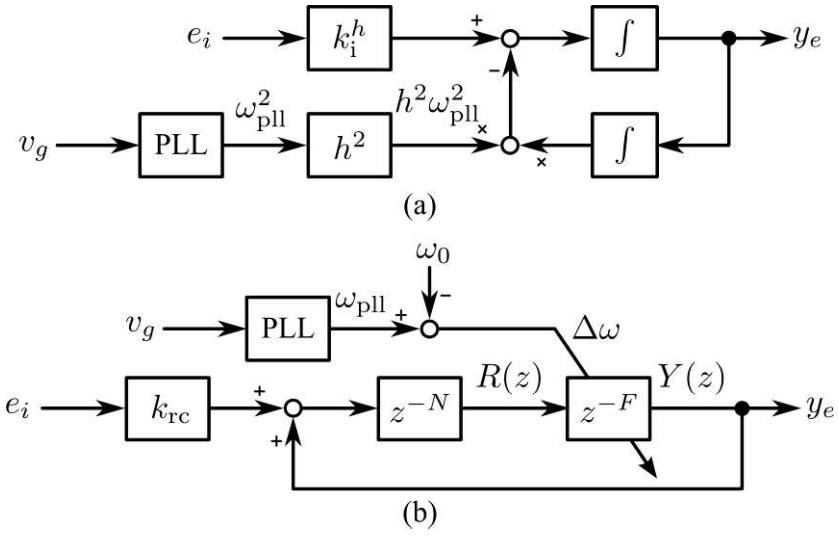

Fig. 5.17. Frequency adaptive periodic current controllers for the GSC: (a) for resonant control and (b) for repetitive control.

The major research background lies in that for grid-connected applications, including PV systems, the grid frequency cannot be maintained always as constant. Hence, the varying grid frequency challenges the control of GSC proposed in this project. As a result, the operation of both PR+RES and PR+RC current controller (when they are digitally implemented in the embedded micro-controller of the GSC) is negatively affected under non-nominal grid frequency conditions. To address this issue, the digital current controllers for the GSC have been modified, where the fractional delay units have been approximated by means of *Lagrange Interpolation Polynomial*, as shown in Fig. 5.17. By doing so, the performance of the periodic current controllers for the GSC is improved, where the control of the GSC becomes immune to grid frequency changes. Fig. 5.18 shows how the Lagrange method is implemented, where the Lagrange Coefficients can be obtained as

$$z^{-F} \approx \sum_{l=0}^{L}\left(z^{-l}H_l\right) \quad \text{with} \quad H_l = \prod_{\substack{i=0 \\ i\neq l}}^{L}\frac{F-i}{l-i}\,.$$

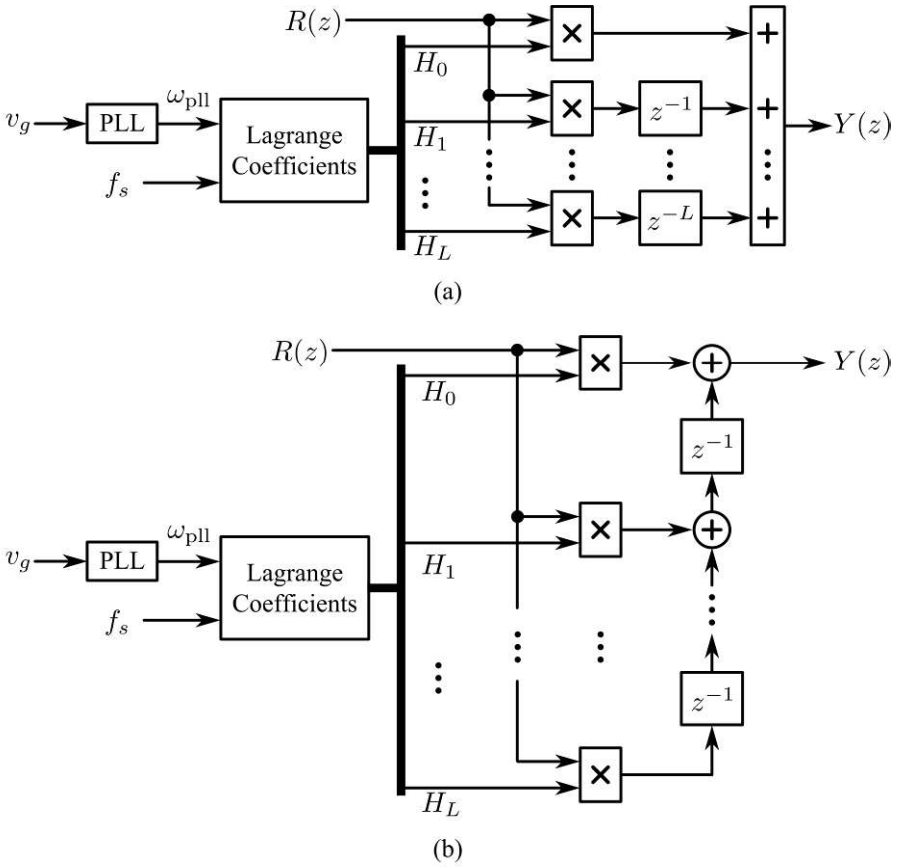

Fig. 5.18. Different implementations of the fractional delay filter, where $z^{-F} = Y(z)/R(z)$: (a) a parallel structure and (b) the Farrow structure.

Some results are presented in Fig. 5.19 for the quality of the injected currents when different current controller are used for current controller without frequency adaptability, and for current controller adopting the proposed frequency adaptive schemes. It is obvious that the frequency adaptive current controllers for the GSC are beneficial for the power quality of the injected currents under different grid frequencies. It can be seen in Fig. 5.19 that with the enhanced frequency adaptive current controllers the Total Harmonic Distortion (THD) of the injected currents can be significantly decreased under non-nominal frequencies and therefore, the new GSC employing frequency adaptive controllers can inject high quality currents.

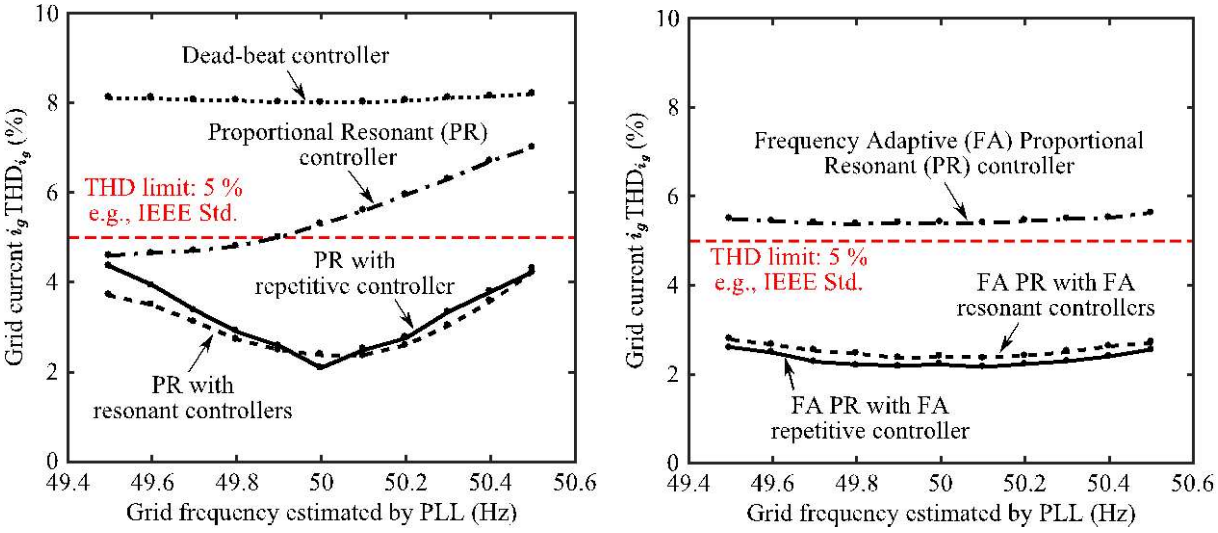

(a) (b)

Fig. 5.19. Results of the GSC single-phase system with different current controllers under a wide range of grid frequency variations: (a) conventional and (b) frequency-adaptive controllers.

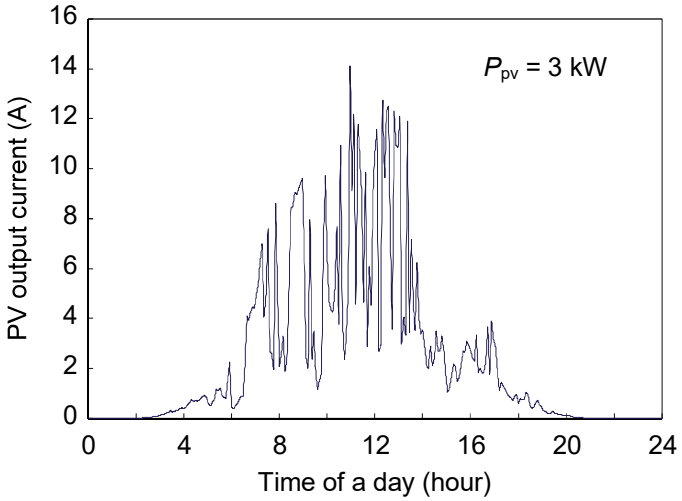

Fig. 5.20. Weather dependence (i.e., intermittency) of the PV systems, indicating the effects on the output current and thus, the injected grid current.

(2) Enhanced current controller for harmonics of PV systems under different operation modes.

Since the PV systems are of high intermittency as shown in Fig. 5.20, the power injected by the GSC PV systems will always be fluctuating. In the case of a high penetration degree of PV systems, the fluctuating power will cause adverse impacts on the entire grid, for instance, harmonics. While under different operation modes, the quality of the injected currents by the GSC may vary. Thus, in this study, the major objective is to identify the root causes of harmonic distortions of single-phase GSC systems. Fig. 5.21 shows the experimental results of a single-phase double-stage GSC system under different operational modes. It can be observed in Fig. 5.21 that the injected power levels (i.e., grid current amplitudes) will affect the current quality. Moreover, reactive power injection will also affect the quality of the injected currents by the GSC.

According to the power balance between PV and the grid, the following have been derived:

$$\tilde{v}_{\mathrm{dc}} \approx \begin{cases} -\int \left[\dfrac{V_{\mathrm{inv}}^{1} I_{g}^{1}}{C_{\mathrm{dc}} V_{\mathrm{dc}}} \cos\left(2\omega_0 t + \varphi - \varphi_1\right) \right] dt & \text{normal operation} \\ -\int \left[\dfrac{V_{\mathrm{g}}^{1} I_{g}^{1}}{C_{\mathrm{dc}} V_{\mathrm{dc}}} \cos\left(2\omega_0 t + \varphi\right) - \dfrac{\omega_0 L_1 \left(I_{g}^{1}\right)^2}{C_{\mathrm{dc}} V_{\mathrm{dc}}} \sin\left(2\omega_0 t\right) \right] dt & \text{abnormal operation} \end{cases}$$

which indicates that the dc-link voltage variations are related to voltage amplitude, current amplitude, DC link capacitance, and DC link voltage level. The relationship has been shown in Fig. 5.22 and Fig. 5.23. Moreover, the variations have a frequency of twice the grid-fundamental frequency. The double-frequency variations will be modulated with the fundamental components, and thus odd-order harmonics will appear in the grid current. Clearly, under different operation conditions (e.g., nominal grid condition with unity power factor and fault ride-through mode with reactive power injection), the current quality will be affected.

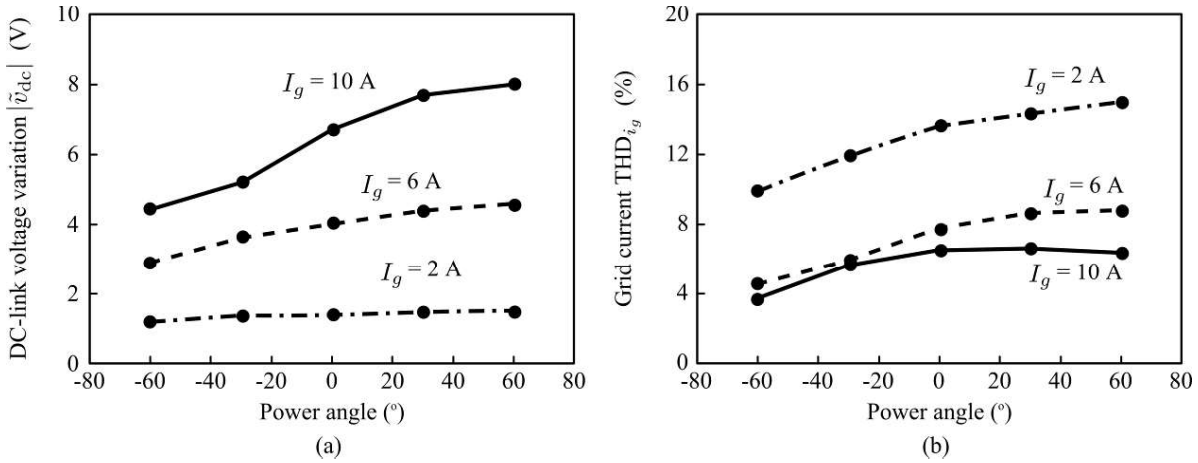

Fig. 5.21. Experimental results for a single-phase double-stage GSC PV system under different power angles and grid current levels with a PR controller (I_g—grid current amplitude): (a) DC-link voltage variation amplitude and (b) THD of the injected grid current.

The basic mechanism of harmonic current injection from a single-phase system has been elaborated above, where the grid voltage quality is assumed to be good enough. However, it should be noted that the grid voltage distortion will definitely affect the current quality. Moreover, the grid synchronization scheme, taking the grid voltage as input, is inevitable for single-phase systems. Thus, the performance of synchronization method might have an impact on the current. For a specific case of PV systems, anti-islanding algorithms are required. Among various islanding detection techniques, the active methods produce a non-sinusoidal current reference. It means that the anti-islanding algorithms for PV systems will also deteriorate the feed-in current to some extent. However, the current controller with harmonic compensators will alleviate this impact. In different applications, the grid-connected inverter systems will operate in various sites and daily changing environmental conditions. Accordingly, the changing solar irradiance will directly affect the PV panel output power. As a result, the injected current level is affected, and also the power quality will change.

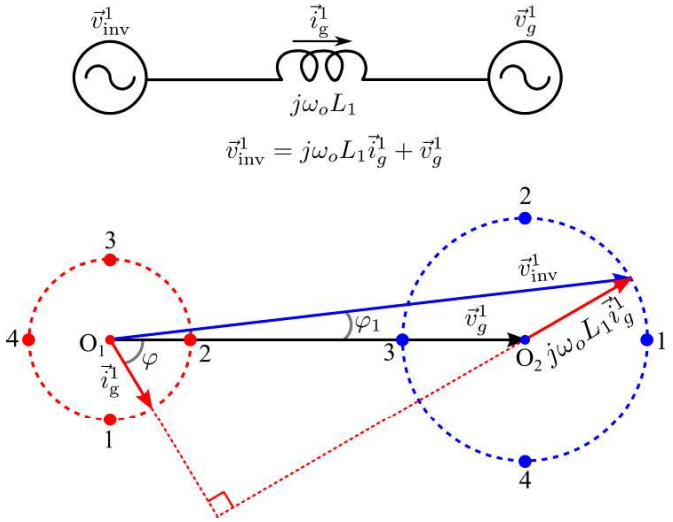

Fig. 5.22. Simplified model and the fundamental frequency phasor diagram of the ac side circuit (*LC*-filter) with a lagging power factor.

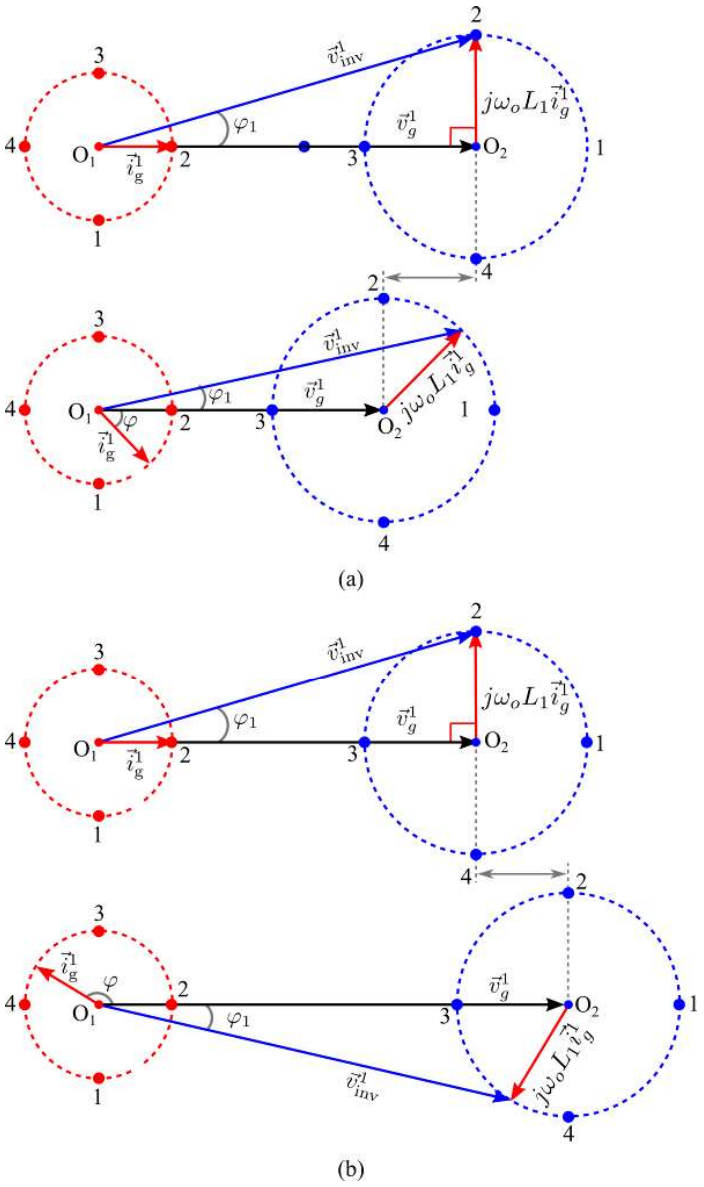

Fig. 5.23. Fundamental frequency phasor diagrams for a single-phase grid-connected system in the case of (a) voltage sag and (b) voltage swell.

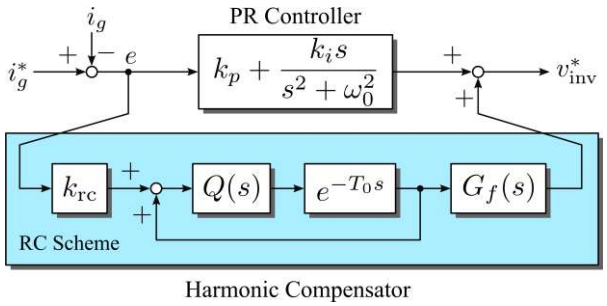

Fig. 5.24. A tailor-made controller (PR current controller with a repetitive-based harmonic controller) for the single-phase grid-connected systems.

In order to maintain the current quality under different operational modes, a tailor-made current controller has been developed, as shown in Fig. 5.24. The tailor-made current controller first employs a fundamental proportional resonant controller to track the fundamental-frequency component, while the plug-in controllers can enhance the tracking accuracy in different operational modes. The results are shown in Fig. 5.25, where it can be observed that the tailor-made controller can maintain the current quality under various conditions in contrast to the results in Fig. 5.21.

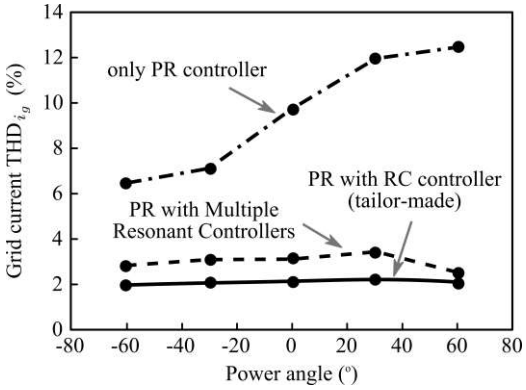

Fig. 5.24. Grid current THD for a single-phase single-stage grid-connected system under different power angles in the normal operational mode with three current control solutions (grid current amplitude I_g = 6 A and grid voltage amplitude V_g = 325 V).

The above outcomes mainly appear in:

[1] Y. Yang, F. Blaabjerg, H. Wang, and M. Simoes, "Power Control Flexibilities for Grid-Connected Multi-Functional Photovoltaic Inverters," IET Renewable Power Generation, vol. 10, no. 4, pp. 504-513, Apr. 2016.

[2] Y. Yang, K. Zhou, and F. Blaabjerg, "Enhancing the Frequency Adaptability of Periodic Current Controllers with a Fixed Sampling Rate for Grid-Connected Power Converters," IEEE Trans. Power Electronics, pp. vol. 31, no. 10, pp. 7273-7285, Oct. 2016.

[3] Y. Yang, K. Zhou, and F. Blaabjerg, "Current Harmonics from Single-Phase Grid-Connected Inverters - Examination and Suppression," IEEE Journal of Emerging and Selected Topics in Power Electronics, vol. 4, no. 1, pp. 221-233, Mar. 2016.

[4] Y. Yang, A. Sangwongwanich, H. Liu, and F. Blaabjerg, “Low Voltage Ride-Through of Two-Stage Grid-Connected Photovoltaic Systems Through the Inherent Linear Power-Voltage Characteristic,” in Proc. of APEC, pp. 3582-3588, Mar. 2017.

[5] E. Afshari, G. R. Moradi, R. Rahimi, B. Farhangi, Y. Yang, F. Blaabjerg, and S. Farhangi, "Control Strategy for Three-Phase Grid-Connected PV Inverters Enabling Current Limitation Under Unbalanced Faults," IEEE Trans. Ind. Electron., vol. 64, no. 11, pp. 8908-8918, Nov. 2017.

[6] L. Hadjidemetriou, P. Demetriou and E. Kyriakides, "Investigation of different fault ride through strategies for renewable energy sources," in Proc. IEEE POWERTECH, Eindhoven, Netherlands, 2015, pp. 1-6.

[7] L. Hadjidemetriou, and E. Kyriakides, "Accurate and efficient modeling of grid tied inverters for investigating their interaction with the power grid,” in Proc. IEEE POWERTECH, Manchester, UK, 2017, pp. 1-6.

[8] L. Hadjidemetriou, E. Kyriakides, and F. Blaabjerg, “A grid side converter current controller for accurate current injection under normal and fault ride through operation,” in Proc. IEEE IECON, pp. 1454–1459, Vienna, Austria, 2013.

[9] L. Hadjidemetriou, L. Zacharia, and E. Kyriakides, "Flexible power control scheme for interconnected photovoltaics to benefit the power quality and network losses of the distribution grid,” in Proc. IEEE ECCE-Asia 2017, Kaohsiung, Taiwan, 2017, pp. 1-6.

[10] Z. Ali, L. Hadjidemetriou, N. Christofides, and E. Kyriakides, "An advanced current controller with improved performance and complexity under abnormal grid conditions,” in Proc. IEEE POWERTECH, Manchester, UK, 2017, pp. 1-6.

[11] Z. Ali, L. Hadjidemetriou, N. Christofides, and E. Kyriakides, “A computationally efficient current controller for simultaneous injection of both positive and negative sequences,” in Proc. IEEE ECCE-Europe (EPE), Warsaw, Poland, 2017, pp. 1-10.

[12] Z. Ali, L. Hadjidemetriou, N. Christofides, and E. Kyriakides, "Diversifying the role of distributed generation grid side converters for improving the power quality of the distribution networks using advanced control techniques,” in Proc. IEEE ECCE, Cincinnati, OH, USA, 2017, pp. 1-8.

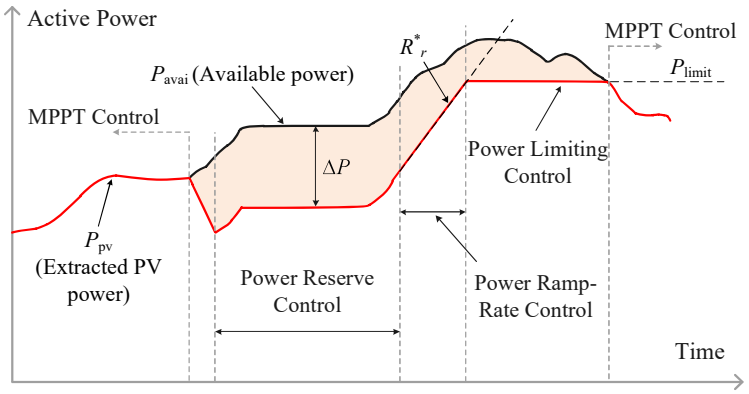

Fig. 5.25. Active power control strategies for grid-connected PV systems defined in the Danish grid code (P_{pv}: PV power, P_{avai}: available power, P_{limit}: the power limit level, R^*_r: the ramp-rate limit, ΔP: the power reserve level.

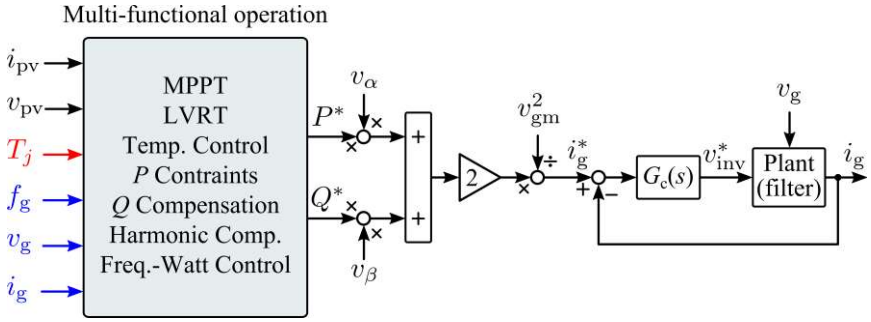

Fig. 5.26. PQ control structure for single-phase PV systems to implement multiple fuctions.

➢ *Development of PQ controllers (for flexible power control)*

To enable profit/energy scheduling control, the flexible active power control for the PV system, where the active power generated by the PV systems has to be able to be regulated upon demands, e.g., during grid frequency deviation, is required. An example of active power control strategies for PV systems introduced in the grid code as it is shown in Fig. 5.25, where various power control functionalities have been defined. In addition, as the PV systems are idle during nights. Reactive power compensation can be obtained through PV systems. Fig. 5.26 shows that how active and reactive powers are controlled in PV systems, which is based on the PQ controllers. As it is oberved, various functions can be achieved using the PQ control system. The following selectively demonstrates the power controllability of PV systems.

(1) Power Limiting Control (PLC) Algorithm

For the power limiting control strategy, the PV system is not allowed to deliver the output power higher than the power limit value P_{limit}. This condition can be easily fulfilled as long as the available PV power is less than the power limit value (i.e., $P_{avai} \leq P_{limit}$) which usually occurs during the low solar irradiance condition. In that case, the typical MPPT operation is employed, where the reference PV voltage v^*_{pv} is set from the MPPT algorithm (e.g., P&O MPPT), to allow the PV system to inject the maximum available power to the grid (i.e., A→B in Fig. 5.27). However, once the available PV power is reaching and exceeding the level of power limit (i.e., $P_{avai} > P_{limit}$), e.g., due to the solar irradiance level increase, the operating point of the PV system in the P-V curve needs to be regulated below the MPP. More specifically, in order to keep the PV power to be constant at a certain value, the operating point of the PV system has to be regulated along the horizontal line during the solar irradiance change (i.e., B→C in Fig. 5.27). This can be achieved by continuously perturbing the reference PV voltage v^*_{pv} towards the left side of the MPP, i.e., $P_{pv} = P_{limit}$, as it is illustrated in Fig. 5.27.

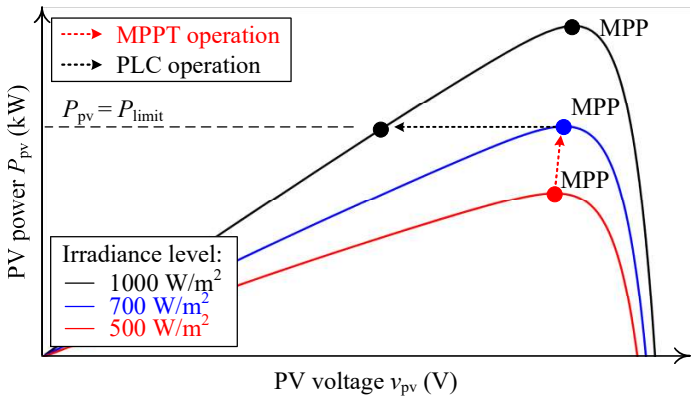

Fig. 5.27. Operational principle of the Power Limiting Control (PLC) algorithm: MPPT mode (A→B) and PLC mode (B→C), where P_{limit} is the power limit.

Fig. 5.28 demonstrates an example of the PLC operation during the day, where the power limit level P_{limit} is chosen as 1.5 kW. Here, two different cases are considered where the PV system operates under a clear day condition in Fig. 5.28(a) and under a cloudy day condition in Fig. 5.28(b). It can be clearly seen in Fig. 5.28(a) that the PV output power follows the maximum available power during the low solar irradiance condition (i.e., $P_{avai} \leq P_{limit}$), while it is kept constant at the set-point once the available PV power exceeds the power limit level (i.e., $P_{avai} > P_{limit}$). Similarly, the power limiting control condition is also achieved during the fluctuating solar irradiance condition in Fig. 5.28(b). In this case, the operating mode is switched between the MPPT and the PLC depending on the solar irradiance condition. In any case, the maximum PV power injection can be limited according to the set-point and the PLC requirement is fulfilled.

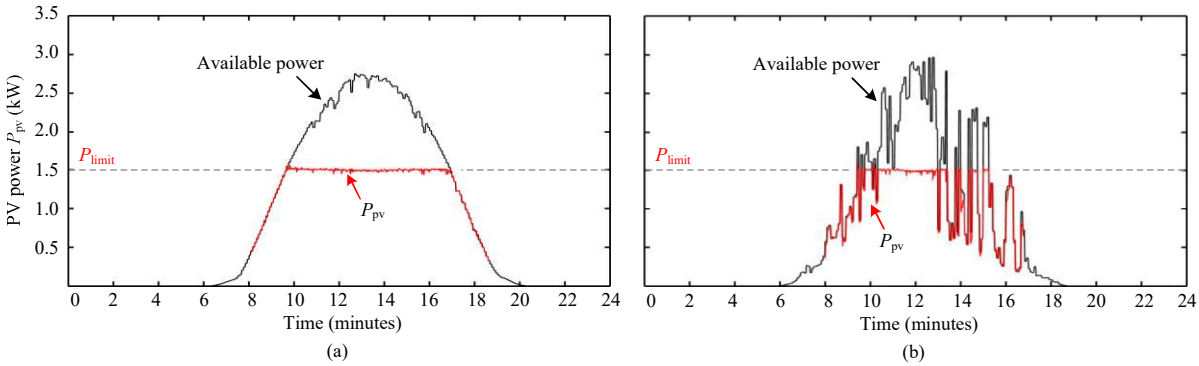

Fig. 5.28. PV output power with the Power Limiting Control (PLC) strategy under: (a) a clear day and (b) a cloudy day irradiance conditions (with an accelerated test to reduce the testing time from 24 hours to 24 minutes), where the power limit level P_{limit} is 1.5 kW.

(2) Power Ramp-Rate Control (PRRC) Algorithm

In the case of the power ramp-rate control, the goal of this control strategy is to regulate the change rate of the PV power to a certain limit R^*_r, instead of an absolute PV power like in the PLC strategy. Therefore, the criterion to reduce (or curtail) the PV power is coming from the change rate of the PV power, which can be calculated as

$$R_r(t) = dP_{pv}/dt$$

As long as the change rate in the PV power is below the maximum limit (i.e., $R_r(t) \leq R^*_r$), the PV system is allowed to operate in the MPPT operation, since the power ramp-rate constraint is fulfilled (i.e., A→B in Fig. 5.29). Nevertheless, during a fast increase in the solar irradiance (e.g., from 700 W/m^2 to 1000 W/m^2), the PV power change rate can exceed the maximum limit and violate the

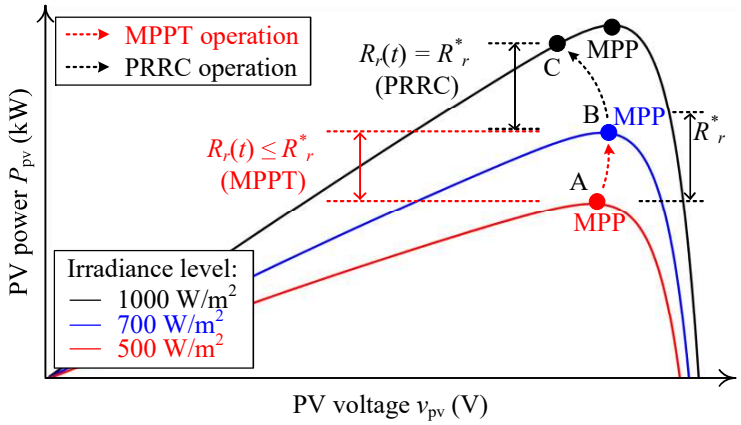

Fig. 5.29. Operational principle of the PRRC algorithm: MPPT mode (A→B) and PRRC mode (B→C), where $R_r(t)$ is the PV power ramp-rate and R^*_r is the ramp-rate limit.

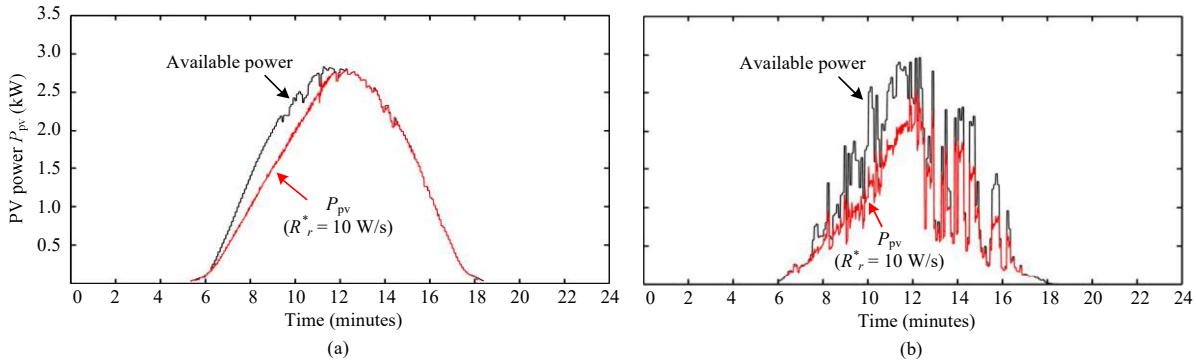

Fig. 5.30. PV output power with the PRRC strategy under: (a) a clear day and (b) a cloudy day irradiance conditions (with an accelerated test to reduce the testing time from 24 hours to 24 minutes), where the ramp-rate limit R^*_r is 10 W/s.

power ramp-rate constraint (i.e., $R_r(t) > R^*_r$). In that case, the extracted PV power needs to be reduced in order to regulate the change rate of the PV power. This can be achieved by perturbing the PV voltage v^*_{pv} towards the left side of the MPP until the PV power change rate is equal to the set point (i.e., $R_r(t) = R^*_r$), as it is shown in Fig. 5.29.

The performance of the PV system with the PRRC strategy is demonstrated in Fig. 5.30(a) with a clear day solar irradiance and ambient temperature condition. The available power and the extracted PV power with the PRRC algorithm are shown in Fig. 5.30(a), where it can be seen that the PV power follows a ramp-changing manner. The corresponding power ramp-rate with the PRRC strategy is shown in Fig. 5.31(a), which verifies that the change rate of the PV power is kept below the maximum limit (i.e., $R_r(t) \le R^*_r$). Another experimental result with a fluctuating solar irradiance (e.g., during a cloudy day) is shown in Fig. 5.30(b). In this case, it is more challenging to control the change rate of the PV power due to the rapid change in solar irradiance condition. It can be seen from the ramp-rate result in Fig. 5.31(b) that the change rate of the PV power can be limited according to the reference in most cases. The PV power ramp-rate limited is only exceeded during very fast transient, where the PRRC algorithm requires a number of iteration to reduce the PV power change rate according to the set-point R^*_r. Nevertheless, the experimental results have confirmed that the PRRC algorithm can effectively control the change rate in the PV power according to the demand.

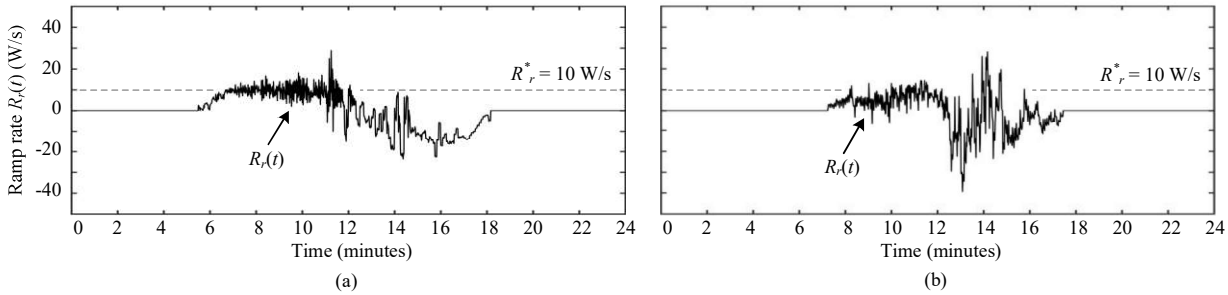

Fig. 5.31. Measured power ramp-rate of the Power Ramp-Rate Control (PRRC) strategy under: (a) a clear day and (b) a cloudy day irradiance conditions (with an accelerated test to reduce the testing time from 24 hours to 24 minutes), where the ramp-rate limit R^*_r is 10 W/s.

(3) Power Reserve Control (PRC) Algorithm

The idea of the power reserve control is to keep the PV output power follow the available PV power dynamic with the power difference corresponding to the amount of power reserve ΔP. The basic concept of this operation can be expressed as

$$P_{pv} = P_{avai} - \Delta P$$

where P_{avai} is the available PV power, P_{pv} is the PV output power, and ΔP is the power reserve level. By doing so, the PV system will be able to support the active power to the grid during the operation with the maximum value corresponding to the power reserve level ΔP.

Actually, the PRC strategy can be seen as a special case of the power limiting control strategy, where the set-point P_{limit} is dynamically changed during the operation in order to provide a constant power reserve. The power limit level employed in the PRC strategy can be calculated by subtracting the available PV power P_{avai} with the required amount of power reserve as: $P_{limit} = P_{avai} - \Delta P$. Therefore, the key of the PRC strategy is to determine (or estimate) the available PV power during the operation. Once the available PV power is known, a similar control algorithm can be employed to reduce the PV output power to a certain level of power limit. Fig. 5.32 illustrates the operational principle of the PRC algorithm where it can be seen that the extracted PV power from the PV system is always kept below the MPP with a certain amount of power reserve.

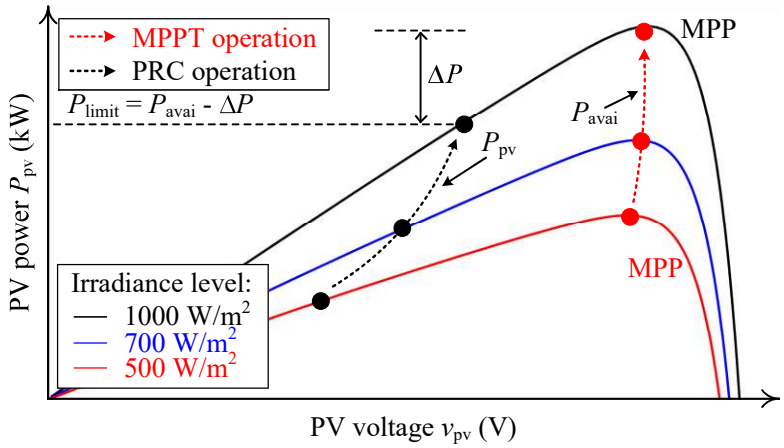

Fig. 5.32. Operational principle of the Power Reserve Control (PRC) algorithm, where P_{avai} is the available PV power and ΔP is the power reserve level.

An example of the PV system with the PRC strategy is shown in Fig. 5.33(a) and (b), where the power reserve level is chosen as 200 W. It can be seen from the results in Fig. 5.33(a) and (b) that the extracted PV power follow the dynamic in the available PV power with the reduced amount corresponding to the power reserve level once the PRC strategy is activated. Accordingly, the power

reserve can be achieved as it is shown in Fig. 5.34. Notably, the fluctuation in the power reserve during the cloudy day condition in Fig. 5.34(b) is due to the fluctuating solar irradiance condition. In that case, the sampling rate of the control algorithm needs to be increased, in order to improve the dynamic of the PRC algorithm. Nevertheless, the PRC algorithm is effective in terms of providing the power reserve following the demand.

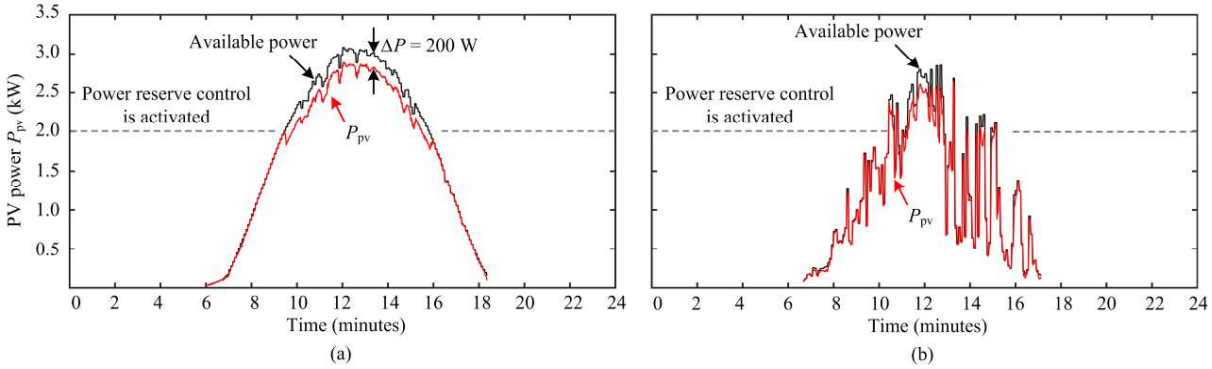

Fig. 5.33. PV output power of the Power Reserve Control (PRC) strategy under: (a) a clear day and (b) a cloudy day irradiance conditions (with an accelerated test to reduce the testing time from 24 hours to 24 minutes), where the reference power reserve level Δ*P* is 200 W and the PRC strategy is activated when P_{pv} > 2 kW.

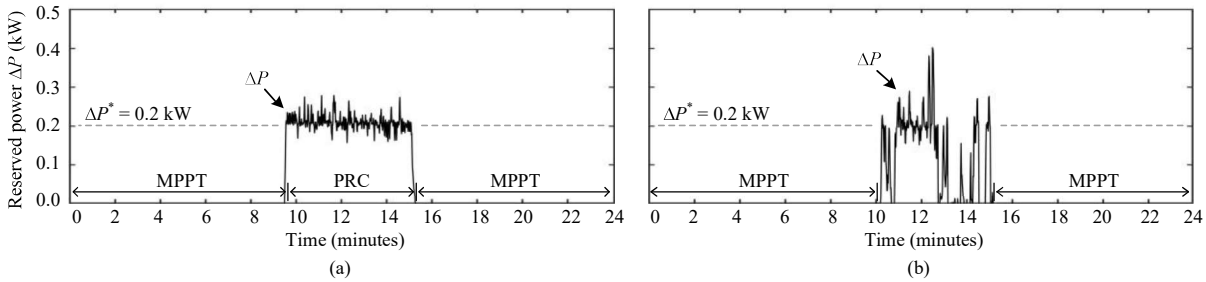

Fig. 5.34. Measured power reserve of the Power Reserve Control (PRC) strategy under: (a) a clear day and (b) a cloudy day irradiance conditions (with an accelerated test to reduce the testing time from 24 hours to 24 minutes), where the power reserve level Δ*P* is 200 W.

The above outcomes mainly appear in:

[1] A. Anurag, Y. Yang, and F. Blaabjerg, “Thermal Performance and Reliability Analysis of Single-Phase PV Inverters with Reactive Power Injection Outside Feed-In Operating Hours,” IEEE J. Emerg. Sel. Top. Power Electron., vol. 3, no. 4, pp. 870-880, Dec. 2015.

[2] Y. Yang, F. Blaabjerg, H. Wang, and M. Simoes, "Power Control Flexibilities for Grid-Connected Multi-Functional Photovoltaic Inverters," IET Renewable Power Generation, vol. 10, no. 4, pp. 504-513, Apr. 2016.

[3] A. Sangwongwanich, Y. Yang, and F. Blaabjerg, “High-Performance Constant Power Generation in Grid-Connected PV Systems,” IEEE Trans. Power Electron., vol. 31, no. 3, pp. 1822-1825, Mar. 2016.

[4] A. Sangwongwanich, Y. Yang, F. Blaabjerg, and D. Sera, “Delta Power Control Strategy for Multistring Grid-Connected PV Inverters,” IEEE Trans. Ind. Appl., vol. 53, no. 4, pp. 3862-3870, Jul.-Aug. 2017.

[5] Y. Yang, E. Koutroulis, A. Sangwongwanich, and F. Blaabjerg, “Pursuing Photovoltaic Cost-Effectiveness: Absolute Active Power Control Offers Hope in Single-Phase PV Systems,” IEEE Ind. Appl. Mag., vol. 23, no. 5, pp. 40-49, Sept.-Oct. 2017.

[6] A. Sangwongwanich, Y. Yang, and F. Blaabjerg, “A Sensorless Power Reserve Control Strategy for Two-Stage Grid-Connected PV Systems,” IEEE Trans. Power Electron., vol. 32, no. 11, pp. 8559-8569, Nov. 2017.

[7] A. Sangwongwanich, Y. Yang, F. Blaabjerg, and H. Wang, “Benchmarking of Constant Power Generation Strategies for Single-Phase Grid-Connected Photovoltaic Systems,” IEEE Trans. Ind. Appl., vol. PP, no. 99, in press, 2018.

➢ *Reliability Analysis*

For grid-connected PV systems, the cost associated with the PV inverter failure is around 59 % of the total system cost. Therefore, the lifetime prediction of PV inverters plays a crucial role in terms of the operational cost assessment, and thus design for reliability.

Lifetime of PV inverter is strongly affected by several aspects such as the hardware design of the inverter (e.g., component selection, cooling design), control strategy (e.g., reactive power injection, power limiting control). In addition, the PV panel also has a significant influence on the reliability of the PV inverter, as it determine the inverter loading. For instance, PV panel degradation and oversizing are the two main aspects that strongly affect the long-term PV power production, whose influence on the inverter lifetime will be addressed in the following. The case study of the installation sites in Denmark and Arizona are used to represent the variation in mission profile of the PV system.

(1) PV panel degradation

In the prior-art work, the impact of PV panel degradations is not taken into consideration in the lifetime evaluation. It is usually assumed that the PV power production and the thermal loading of the PV inverter are repeated yearly for certain installation sites. However, this assumption is not very accurate in practical applications, as it is well known that the PV panels degrade during operation. More precisely, the aged PV panels will produce less energy than the newly installed ones. This implies that the thermal loading and thereby the LC of the PV inverter will be reduced over time (under the same mission profile).

For instance, an encapsulant discoloration, which is one of the most commonly-reported failure modes in PV panels, usually leads to a linear degradation of PV panels where the PV power production decreases linearly over time. The PV panel degradation rate can also be determined from real-field measurements. In that case, a linear degradation characteristic is usually assumed, where the degradation profile is obtained from the real-field measured data. In this study, the degradation rate of 0.15%/year in Denmark and 1%/year in Arizona are used. The yearly degradation profile of the PV panels at these locations is shown in Fig. 5.35.

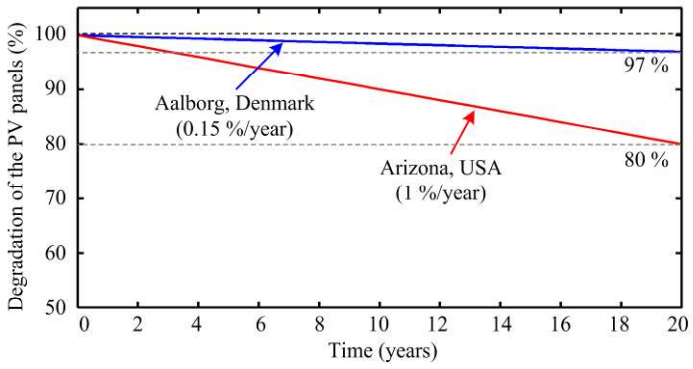

Fig. 5.35. Degradation profiles of the PV panels installed in Denmark and Arizona with the degradation rate of 0.15 %/year and 1 %/year, respectively.

The junction temperature variation is a consequence of the power device loading. In this regards, the impact of PV panel degradations can be observed in the junction temperature variations in the PV inverters, as it is shown in Figs. 5.36 and 5.37. The mean junction temperature T_{jm} of the PV inverter in Arizona reduces significantly after 5 years of operation, due to the high degradation rate of the PV panels. It can be seen from Fig. 5.37 that the mean junction temperature in Arizona is approximately 3°C lower compared to the first year, while the reduction in the mean junction temperature is very small in Denmark. Similarly, the cycle amplitude of the junction temperature ΔTj is also reduced significantly after 5 years of operation for the PV inverter installed in Arizona.

The yearly LC of the power device is calculated for an operation of 20 years in order to observe the impact of the panel degradation in the long-term LC. It can be seen from Fig. 5.38 that the yearly LC of the PV inverter installed in Arizona reduces significantly during the entire operation, where a reduction of 82% from the initial LC has been observed. In contrast, the LC of the PV inverter in Denmark only reduces by 20% over an operation of 20 years due to the lower panel degradation rate.

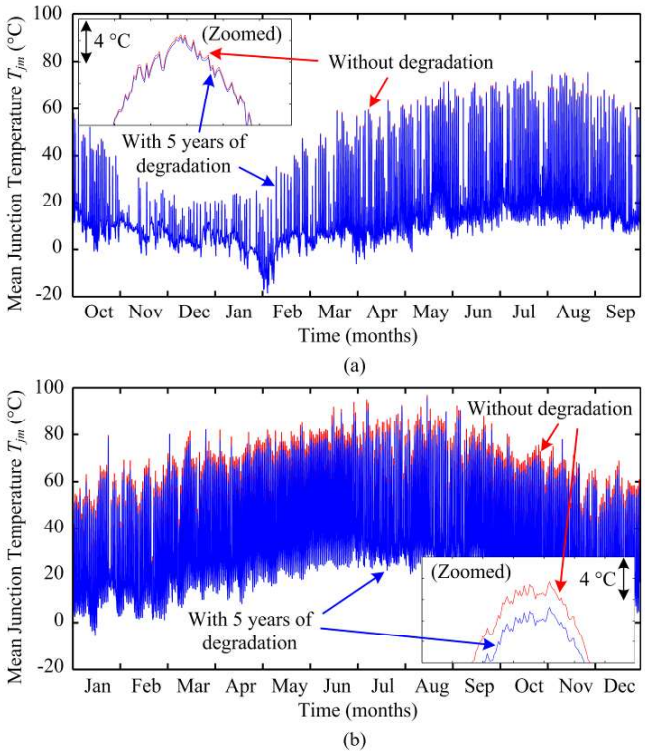

Fig. 5.36. Mean junction temperature T_{jm} of the power device under a yearly mission profile in: (a) Denmark and (b) Arizona.

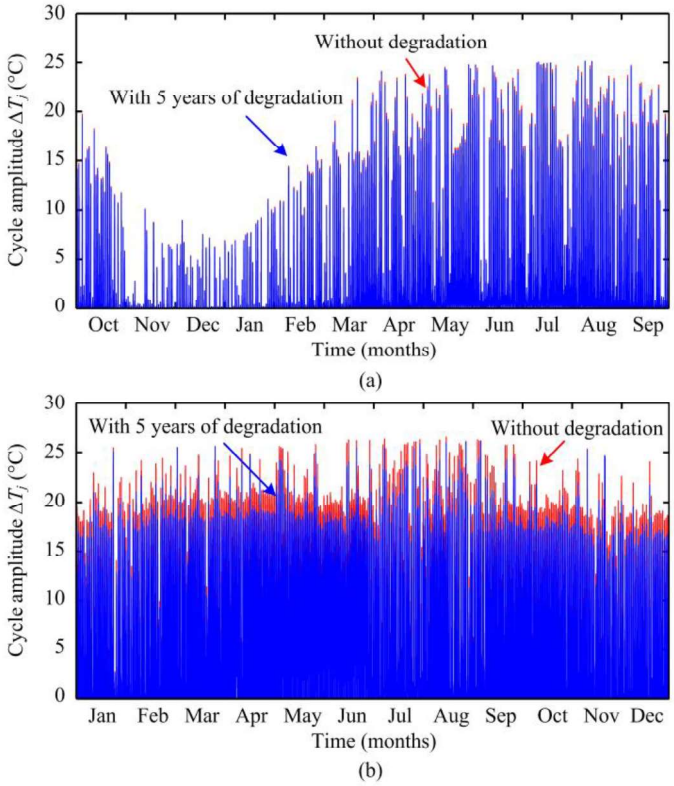

Fig. 5.37. Cycle amplitude ΔT_j of the device junction temperature under a yearly mission profile in: (a) Denmark and (b) Arizona.

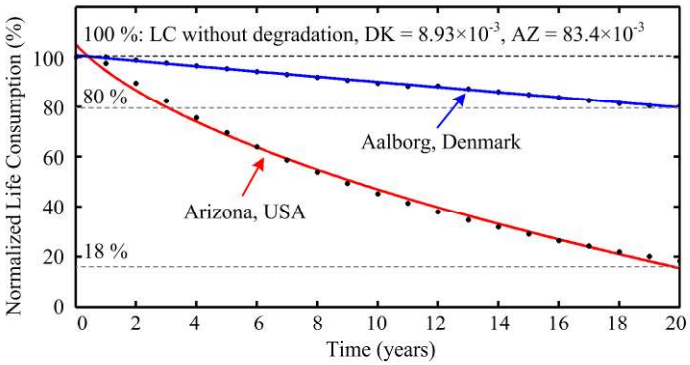

Fig. 5.38. Normalized yearly life consumption of the power device during 20 years of operation in Denmark and Arizona.

The unreliability functions of the PV inverter installed in Denmark and Arizona are shown in Figs. 5.39 and 5.40, respectively. The unreliability function of one power device is indicated by the blue plot together with the B_x lifetime of the power device (e.g., the time when x % of a population is failed). For instance, the B_{10} lifetime of the PV inverter installed in Arizona is underestimated by 54 % (7 years), if the panel degradation is not considered. This means that the PV inverter in the case when without considering panel degradation is expected to be replaced approximately twice as many as the case where the panel degradation is considered. This will inevitably lead to a significant overestimation in the maintenance costs of PV inverters during the entire operation.

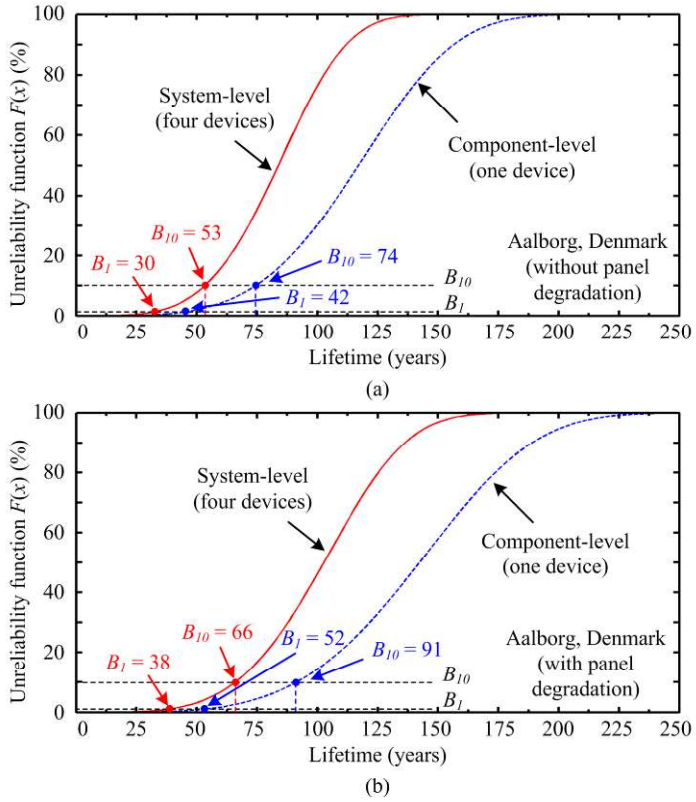

Fig. 5.39. Unreliability function of the PV inverter installed in Denmark: (a) without panel degradation and (b) with panel degradation, where blue lines indicate component-level and red lines indicate system-level reliability.

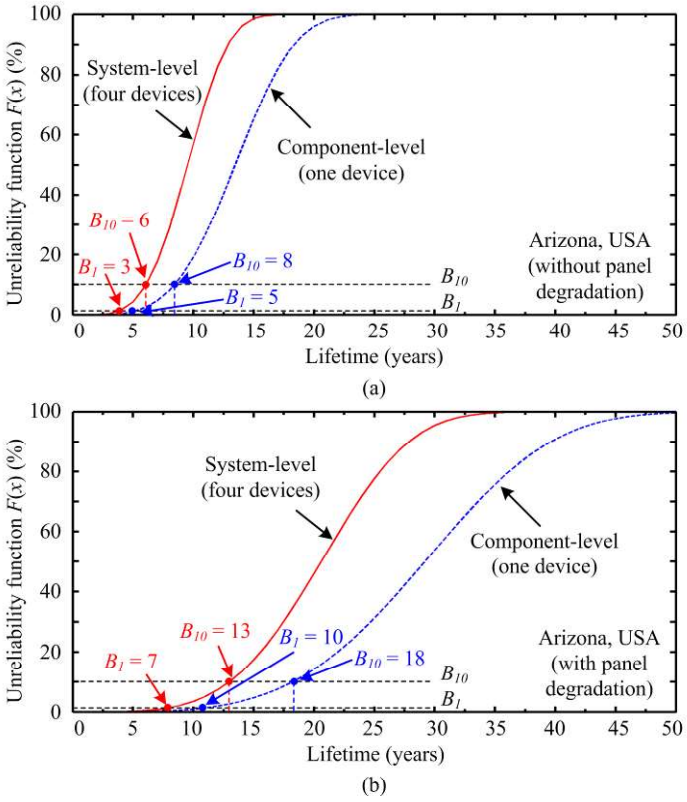

Fig. 5.40. Unreliability function of the PV inverter installed in Arizona: (a) without panel degradation and (b) with panel degradation, where blue lines indicate component-level and red lines indicate system-level reliability.

(2) PV panel oversizing

One commonly used solution to reduce the cost of solar energy is to oversize the PV arrays (the cost of PV modules is relatively low), where the rated power of the PV arrays is intentionally designed to be higher than the rated power of the PV inverter. By doing so, the PV inverter will operate close to its rated power during a larger proportion of time, and thus more PV energy can be captured during the non-peak production periods. The PV power extraction during a day with oversized PV arrays is illustrated in Fig. 5.41.

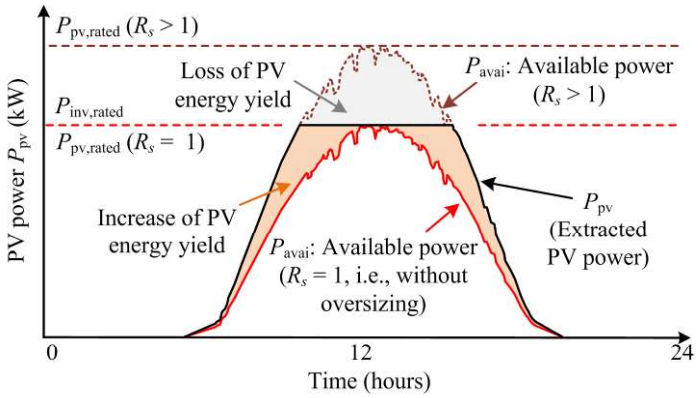

Fig. 5.41. PV power extraction with oversized PV arrays (P_{avai}: available PV power, P_{pv}: extracted PV power, $P_{pv,rated}$: PV array rated power, $P_{inv,rated}$: PV inverter rated power, $R_s = P_{pv,rated}/P_{inv,rated}$: sizing ratio).

However, oversizing the PV array will inevitably affect the operation and the loading, and thus the inverter reliability and lifetime. For instance, the PV inverters with oversized PV arrays will have longer operating time at high power production than those without oversized PV arrays under the

same mission profile (i.e., solar irradiance and ambient temperature) following Fig. 5.41. This will increase the thermal stresses of the components (e.g., power devices and capacitors), challenging their reliability. In that case, oversizing PV array may increases operational and maintenance cost of the PV inverter and results in a negative impact on the overall PV energy cost.

This project investigates the impacts of the PV array sizing on the PV inverter reliability and lifetime. The analysis includes a lifetime evaluation of reliability-critical components in the system such as power devices and capacitors, where the lifetime evaluation process is illustrated in Fig. 5.42.

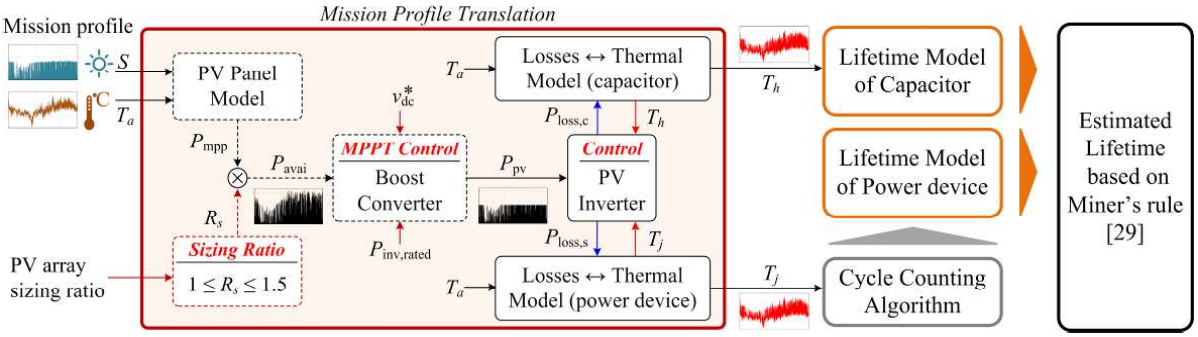

Fig. 5.42. Mission profile-translation diagram of a single-phase PV system, where the PV array-sizing ratio R_s is considered.

In order to investigate the impacts of PV array sizing on the inverter lifetime, the thermal loading of the power devices (i.e., the mean junction temperature T_{jm} and the cycle amplitude ΔT_j) and the capacitors (i.e., the hotspot temperature T_h) in the PV inverter installed in Denmark and Arizona are shown in Figs. 5.43 and 5.44, respectively. Two cases with R_s = 1 (i.e., non-oversized PV arrays) and R_s = 1.4 (i.e., oversized PV arrays) are considered. It can be seen from Fig. 5.43 that the PV inverter installed in Denmark with oversized PV arrays (i.e., R_s = 1.4) has a strong increase in the thermal loading compared to the case where R_s = 1, especially during November through February (when the solar irradiance level is low). The impact of oversizing PV arrays is less pronounced with the PV system installed in Arizona, where only a small increase in the thermal loading of the PV inverter is observed in Fig. 5.44. This is due to the fact that the PV inverter installed in Arizona with R_s = 1.4 mostly operates in the power limiting mode (i.e., P_{pv} = $P_{inv,rated}$) because of the high average solar irradiance level through the year. In that case, oversizing the PV array will not significantly increase the PV power production and thus the thermal loading of the components in the PV inverter.

Further, the life consumption during one-year operation of power devices and capacitor of the PV inverter with different sizing rations under the mission profile in Denmark and Arizona are shown in Figs. 5.45 and 5.46, respectively. The impact of oversizing on the LC is significant with the mission profile in Denmark, where the LC increases considerably as R_s increases. In contrast, the LC of the PV inverter installed in Arizona is less affected by the sizing ratio of the PV arrays. In this case, the LC only increases slightly, and it saturates around 1.5 times of the initial LC (i.e., LC without oversizing) for the power device and 1.4 times of the initial LC for the capacitor. This is simply due to the mission profile characteristics in Arizona, where the solar irradiance is relatively high throughout the year. Thus, oversizing the PV arrays can easily lead to a power limiting operation, due to the maximum capability of the PV inverter. As a consequence, only a small increase in the PV power production is obtained, and thus the impact on the LC of the PV inverter is less significant compared to that in Denmark.

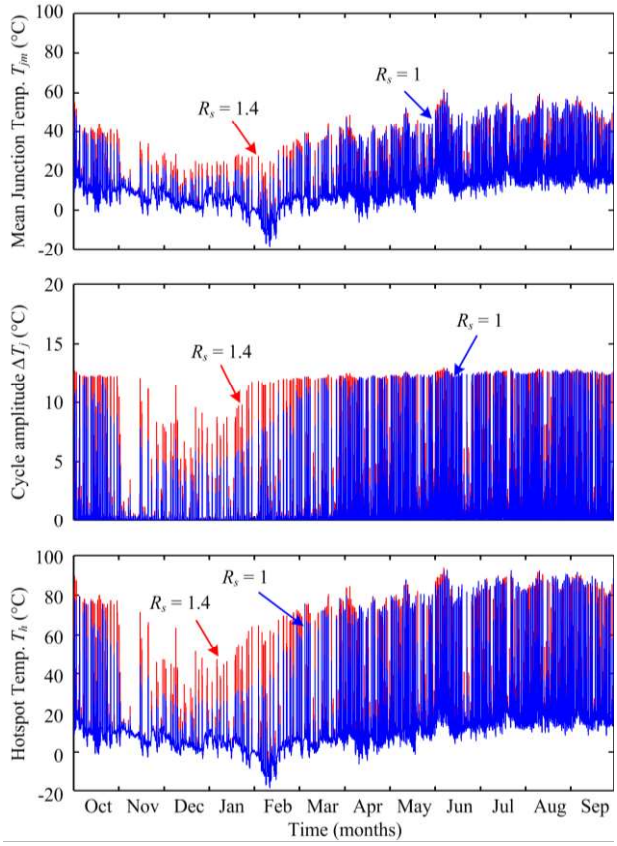

Fig. 5.43. Mean junction temperature T_{jm}, cycle amplitude ΔT_j of the power device, and hotspot temperature of the capacitor T_h under a mission profile in Denmark with two sizing ratios (blue plot: R_s = 1, red plot: R_s = 1.4).

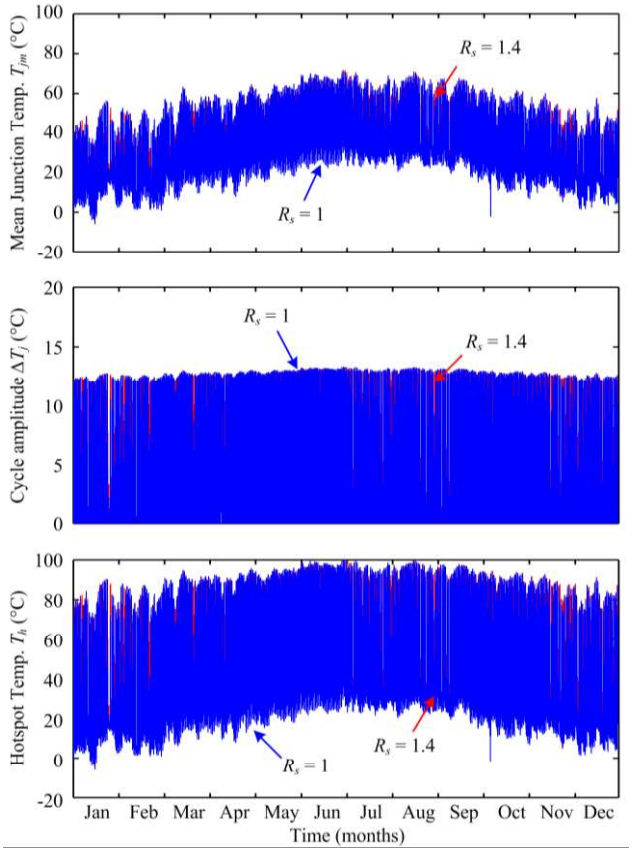

Fig. 5.44. Mean junction temperature T_{jm}, cycle amplitude ΔT_j of the power device, and hotspot temperature of the capacitor T_h under a mission profile in Arizona with two sizing ratios (blue plot: R_s = 1, red plot: R_s = 1.4).

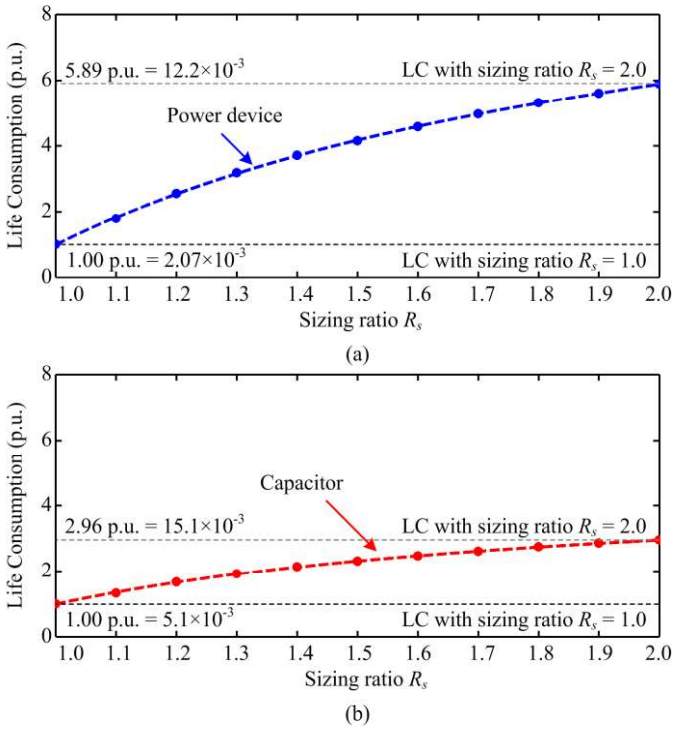

Fig. 5.45. Normalized life consumption of components in PV inverters with different sizing ratios *Rs* for the mission profile in Denmark: (a) power device and (b) capacitor.

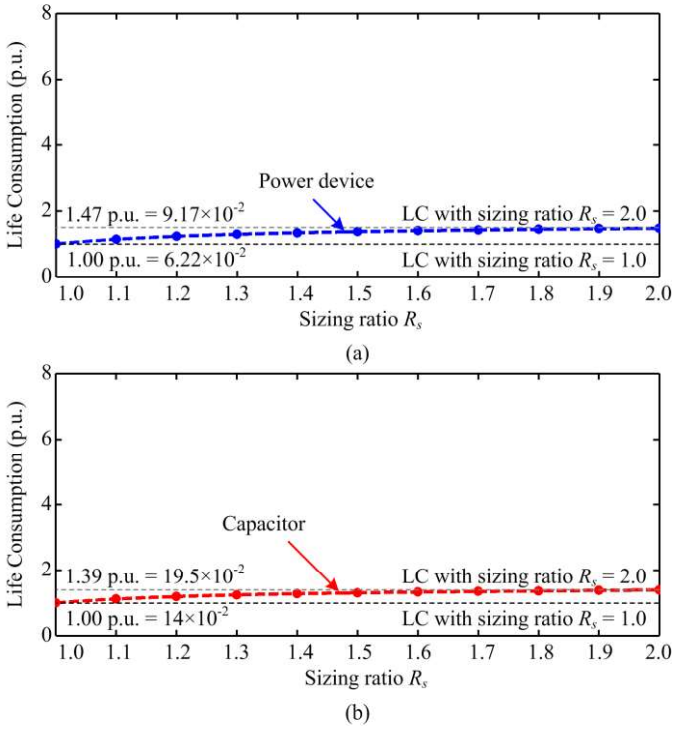

Fig. 5.46. Normalized life consumption of components in PV inverters with different sizing ratios *Rs* for the mission profile in Arizona: (a) power device and (b) capacitor.

The B_{10} lifetime of the PV inverter with different sizing ratios for the two mission profiles is summarized in Fig. 5.47, where it can be seen that the B_{10} lifetime of the PV inverter in Denmark decreases considerably as the sizing ratio R_s increases. As it has been discussed previously, the full-bridge module is the main life-limiting sub-system in this case. In contrast, the impact of the sizing ratio R_s is less significant in the case of the mission profile in Arizona. For example, only a small reduction in the PV inverter lifetime is observed (i.e., less than one year, which is corresponding to 20% reduction) when the sizing ratio of the PV system is increased from R_s = 1 to R_s = 1.4. When the sizing ratio is further increased from R_s = 1.4 to R_s = 2, the B_{10} lifetime of the PV inverter remains

almost constant at B_1 = 4 years (e.g., the lifetime difference is less than a year). In this case, it can be clearly seen from the results in Fig. 5.47(b) that the dc-link is the critical part in the PV inverter. In order to improve the reliability of the overall system, the cooling system of the capacitor may need to be redesigned (e.g., using active cooling method).

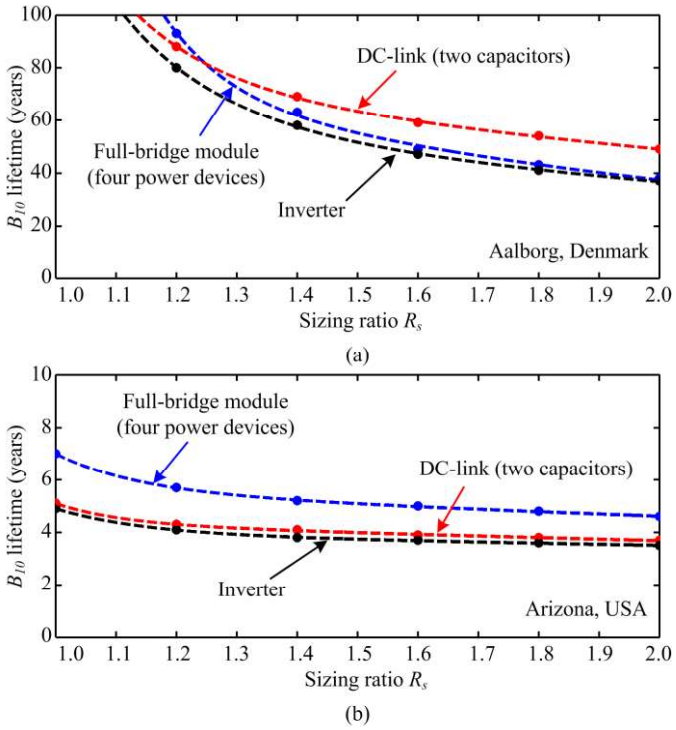

Fig. 5.47. B_{10} lifetime of the PV inverter with different sizing ratios for the mission profile in: (a) Denmark and (b) Arizona.

The above outcomes mainly appear in:

[1] A. Anurag, Y. Yang, and F. Blaabjerg, “Thermal Performance and Reliability Analysis of Single-Phase PV Inverters with Reactive Power Injection Outside Feed-In Operating Hours,” IEEE J. Emerg. Sel. Top. Power Electron., vol. 3, no. 4, pp. 870-880, Dec. 2015.

[2] Y. Yang, F. Blaabjerg, H. Wang, and M. Simoes, "Power Control Flexibilities for Grid-Connected Multi-Functional Photovoltaic Inverters," IET Renewable Power Generation, vol. 10, no. 4, pp. 504-513, Apr. 2016.

[3] A. Sangwongwanich, Y. Yang, and F. Blaabjerg, “High-Performance Constant Power Generation in Grid-Connected PV Systems,” IEEE Trans. Power Electron., vol. 31, no. 3, pp. 1822-1825, Mar. 2016.

[4] Y. Yang, H. Wang, A. Sangwongwanich, and F. Blaabjerg, “Design for reliability of power electronic systems,” Chapter in Power Electronics Handbook, M. H. Rashid (editor), 2018.

[5] A. Sangwongwanich, Y. Yang, D. Sera, and F. Blaabjerg, “Impacts of PV Array Sizing on PV Inverter Lifetime and Reliability,” in Proc. of ECCE, pp. 3830-3837, Oct. 2017.

[6] A. Sangwongwanich, Y. Yang, D. Sera, and F. Blaabjerg, “Lifetime Evaluation of Grid-Connected PV Inverters Considering Panel Degradation Rates and Installation Sites,” IEEE Trans. Power Electron., vol. 33, no. 2, pp. 1225-1236, Feb. 2018.

[7] E. Gurpinar, Y. Yang, F. Iannuzzo, A. Castellazzi, and F. Blaabjerg, “Reliability-Driven Assessment of GaN HEMTs and Si IGBTs in 3L-ANPC PV Inverters,” vol. 4, no. 3, pp. 956-969, Sept. 2016.

[8] Y. Yang, A. Sangwongwanich, and F. Blaabjerg, “Design for reliability of power electronics for grid-connected photovoltaic systems,” CPSS Trans. Power Electron. Appl., vol. 1, no. 1, pp. 92-103, Dec. 2016.

Dissemination of results

The project has resulted in many achievements in terms of publications in journals and conferences, special sessions at conferences, presentations at universities, and further projects. In total, there have been more than 20 journal publications, around 20 conference papers (presentations), 2 chapters, and 1 monograph (contracted) under the PV2GRID. Additionally, one special session was organized at the International Future Energy Electronics Conference (IFEEC 2017 – ECCE Asia) in Kaohsiung, Taiwan, where we focused on the active power control strategies for PV systems. A conference tutorial is planned to summarize the major achievements in this project. One workshop has been held in Aalborg, and one will be done at UCY, where all the results of PV2GRID will be further disseminated.

Publications can be found at:
http://vbn.aau.dk/en/projects/pv2grid(55294bc8-7e7b-4f8b-9bfd-bfe2a11bcf30).html
http://www.kios.ucy.ac.cy/pv2grid/index.php/dissemination

6. Project conclusion

As a conclusion, the project has been running satisfactorily. Through the project, the collaborators have developed many advanced control strategies to enable grid-friendly PV systems and thus smoothly PV to GRID (PV2GRID). More importantly, the project highlighted the major concerns, when integrating a large-scale of PV systems, which is the trend and demand for sustainably societies. Hardware setups have also been built up, which will be used for future applications and projects. However, since Quantum Corporation was not funded, the cost-benefit analysis and the business model for the GSC system are not finalized yet. Additionally, since the start dates of the project at AAU and UCY were different. One workshop at UCY is delayed.

7. Future work

Although many advanced control strategies have been developed for the GSC in this project, there is much more work for grid-friendly PV systems. In the future, an even higher penetration level of PV systems will further challenge the power grid, which will be power electronic-dominant. In that case, the advanced control strategies may be promising solutions. However, this project only explored the full-bridge converters. Advancements in power electronic converters together with those control schemes will add more values. Nevertheless, as highlighted in this project, efficiency and reliability are still of high interest. The developed design for reliability approach that was applied to the GSC systems will be one essential means to reduce the cost of PV energy. Furthermore, applications of emerging power devices in advanced GSC systems are also important. In all, the results of the PV2GRID project will enable more research at Aalborg University.

The deliverables related to the profit/energy scheduling algorithms and business model (D6.1 and D8.2) will be finalized by UCY in March. Other final reporting at UCY (D1.2, D1.3, and D2.5) will be completed also in March 2018. AAU will contribute to the reporting.

Annex

Links to the project at Aalborg University and the University of Cyprus are:

http://vbn.aau.dk/en/projects/pv2grid(55294bc8-7e7b-4f8b-9bfd-bfe2a11bcf30).html
http://www.kios.ucy.ac.cy/pv2grid/